IRANIAN JOURNAL OF PHYSICS RESEARCH

Iranian Journal of Physics Research, Vol. 6, No. 3, 2006

High-temperature superconductors, as seen through the eyes of neutrons

Z Yamani

Canadian Neutron Beam Centre, National Research Council, Chalk River Laboratories, Chalk River, ON K0J 1J0, Canada Electronic E-mail: Zahra.Yamani@nrc.gc.ca

(Received 25 March 2006 ; accepted 1 July 2006)

Abstract

Neutron scattering is proved to be a vital probe in unveiling the magnetic properties of high temperature superconductors (HTSC). Detailed information about the energy and momentum dependence of the magnetic dynamics of HTSC have been obtained directly by this technique. Over the past decade by improving the crystal growth methods, large and high quality single crystals of HTSC, which are essential for a neutron scattering experiment, have become available. The results of neutron scattering measurements on such crystals have considerably enhanced our understanding of the magnetism in HTSC both in the superconducting (SC) and normal states. In this review, the neutron scattering results on two main HTSC families, $La_{2-x}Sr_xCuO_4$ (LSCOx) and $YBa_2CuO_3O_{6+x}$ (YBCO6+x), are considered with an emphasis on the most prominent properties of these materials that are now widely accepted. These include the presence of strong antiferromagnetic (AF) fluctuations even in optimally doped region of the phase diagram, neutron resonance peak that scales with SC transition temperature, T_c, incommensurate magnetic fluctuations (stripes), and a pseudogap in the normal state of underdoped materials.

Keywords: superconductivity, $La_{2-x}Sr_xCuO_4$, $YBa_2CuO_3O_{6+x}$, neutron scattering, magnetic excitations

1. Introduction

Superconductivity was first discovered [1] in 1911 by Kamerlingh Onnes. He succeeded in liquifying helium gas in 1908, and thus was able to reach temperatures just a few degrees above absolute zero for the first time. He found that mercury has zero electrical resistance below 4.2 K. Some other metals also showed the same effect but at different temperatures. He also discovered the existence of a critical magnetic field [2] and a critical current at which superconductivity was destroyed. Another historical discovery about superconductivity was made by Meissner and Oschenfeld in 1933 [3]. They found that superconductors not only have zero resistance below a transition temperature, T_c, but also expel a modest magnetic field from inside.

A successful theory explaining microscopic properties of superconductors became available only forty six years after the first observation of superconductivity. This was partially because the quantum theory of normal metals was not available for two decades. Also, it was not until 1934 that the Meissner effect was observed. After the recognition of concepts such as phonons, Pauli exclusion principle (Fermi-Dirac statistics), considering further experimental clues such as the isotopic effect due to electron-phonon interaction, and by taking into account the influence of electronic screening processes, Bardeen, Cooper, and Schrieffer (BCS) were able [4] to develop their microscopic theory of superconductivity in 1957. They found that the presence of ions, makes possible a net attractive interaction between a pair of electrons whose energy difference is less than a characteristic phonon energy and that the normal state Fermi surface could become unstable at low temperatures to the formation of pairs of electrons of opposite spin and momentum (Cooper pairs) because of this net attraction. The BCS theory was quickly successful in explaining all existing phenomena and predicting new ones in conventional superconductors.

T_c of superconductors resulting from electron-phonon interaction calculated based on BCS theory was found to be less than 30 K [2]. This was explained by the fact that the deriving interaction (electron-phonon) itself is weak. Because of this result and the low T_c's observed experimentally for metal and alloys, for a long time it was believed that there would be no SC matter with T_c higher than 30 K. However, the discovery [5] of a Lanthanum-based oxide superconductor, $La_{2-x}Ba_xCuO_4$ (LBCOx) which exhibited both zero resistance and the Meissner effect around 30 K by Bednorz and Muller in 1986 started a new era in superconductivity research. Soon after this discovery, superconductivity was also observed [6] in YBCO6+x at temperatures ($T_c \sim 90$ K) higher than liquid nitrogen. This made it clear that a

revolution in superconductivity had begun. In the following six years, even higher transition temperatures became [7] available in Bi-based (T_c=120 K), and Hg-based (T_c=134 K and 165 K at very high pressures) cuprates (see figure 1(a)). In addition to such high T_c's, another surprising feature about HTSCs is that superconductivity occurs in a family of ceramic oxides that are very poor metals with low density of free charge carriers compared to normal metals.

While the standard BCS theory works perfectly for the conventional low temperature superconductors with an isotropic gap (s-wave symmetry), it falls short in explaining HTSC cuprates[1]. Since the discovery of HTSC, numerous studies have been made theoretically to elucidate the mechanism of the superconductivity and many exotic theories such as marginal Fermi liquid, anyon superconductivity, resonance valence bond theory (spin-charge separation theory), and antiferromagnetic (AF) fluctuation theory have been proposed [10]. However, in spite of much effort, the origin of the superconductivity in HTSC materials is still unclear and even some of their basic properties (for example in the normal state) are only poorly understood. For example, although Cooper pairs[2] are formed [12] in the superconducting state in HTSCs, many experiments have now provided compelling evidence supporting a gap with a predominantly d-wave ($d_{x^2-y^2}$) symmetry [13].

In spite of the fact that a microscopic explanation that is in any way comparable to the BSC theory for conventional superconductors is still lacking, there are some conclusions that could be drawn from the experimental research independent of a such a model. These include the following. They have at least one CuO_2 plane in their unit cell which is built from a sequence of CuO_2 planes separated by block layers playing the role of charge reservoir; display highly anisotropic electrical and magnetic properties; exhibit superconductivity as a result of the formation of Cooper pairs in a singlet spin-state[3]; and finally, it is generally agreed that the normal state of the cuprates where quantum spin dynamics plays a key role (including the pseudogap for underdoped and strange metal behaviour for optimally doped), from which superconductivity emerges, is either not a Fermi liquid or if it is, its properties are very different from a simple metal.

The phase diagram of HTSC, shown in figure 1(b) schematically, is very rich and complex and contains many states of matter[4]. In fact, it is this diverse behaviour (metallic, insulating, magnetic, SC and possibly some unknown phases of matter) exhibited by cuprates that makes them exciting. At zero doping (undoped) and low temperatures, the system is an AF insulator, with an array of localized Cu spins which alternate in sign throughout the lattice [14]. In this regime with planar Cu in Cu^{+2} state, the dominant interaction between electrons is such that having two electrons on a site costs a lot of energy. Since every site is occupied by one electron, nothing can move without creating a doubly occupied site. Hence AF insulating behavior appears. By increasing hole density, antiferromagnetism is gradually destroyed until a critical doping concentration, x_C, is reached, above which superconductivity appears. One can increase the number of holes in the CuO_2 planes by different means such as cation substitution and oxygen doping. The resulting holes on the planar oxygen sites bond with the nearby Cu spins, making it possible for the other Cu spins to move while destroying the long range AF correlations found in the insulator. Although, above x_C no long range AF ordering exists, the itinerant but nearly localized Cu spins display strong AF correlations even for systems at doping levels which exceed that at which T_c is maximum (optimally doped), the so-called overdoped materials. T_c rises with further increasing hole doping through the underdoped regime, reaches a peak and then falls away again at higher doping (overdoped). Superconductivity persists up to a certain hole concentration above which a normal metal behavior is observed, see figure 1(b).

The optimally doped regime exhibit many properties that are differ from the predictions of the Fermi liquid theory, the standard theory of weakly interacting electrons that is the cornerstone of our understanding of metals[5]. In the overdoped regime, on the right-hand side of the SC dome in figure 1(b), the copper oxides behave more like ordinary metals, including exhibiting T^2 resistivity [16] and angular magnetoresistance oscillations that confirm the existence of a Fermi surface consistent with the predictions of conventional single-electron band theory. Underdoped HTSC materials, show some unusual and interesting properties in their normal state which does not exist in the overdoped region. The most prominent difference between the underdoped and overdoped materials is perhaps the existence of a "pseudogap" in underdoped regime. In this regime, a variety of crossover phenomena are observed at temperatures higher than T_c in which various

1. Some ingredients of the BCS theory are known to be applicable [8]. The semiphenomenological Ginzburg–-Landau theory, with the proper modifications to account for the anisotropy, also applies to HTSC [9]. For example, it is known that HTSC materials are type-II superconductors [9].

2. Hall effects measurements have shown [11] that in HTSC materials, charge carriers are holes.

3. Although the nature of the pairing mechanism is unknown, one can rule out a electron-phonon interaction due to the small or zero isotope effect. This suggests that the Cooper pair formation must either be all electronic in nature or involve phonons in a much more sophisticated way than in BCS.

4. All of these properties depend strongly on defects, disorder, impurities and small changes in chemical doping presenting a challenging problem in cuprates containing more than three elements.

5. Perhaps the most famous property is the d.c. electrical resistivity that has a linear temperature dependence [15] rather than T^2 expected for electrons scattering from one another in simple metals.

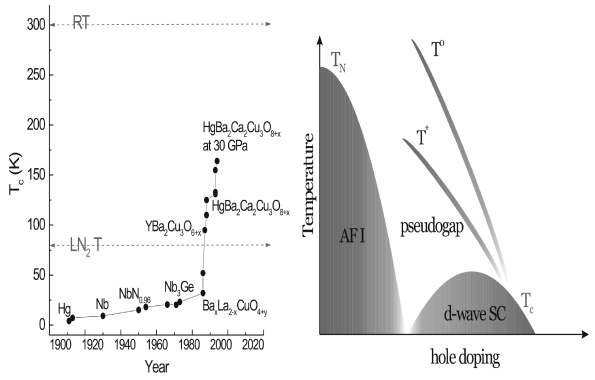

Figure 1. (a) T_c vs. year of discovery. In less than 10 years from discovery of HTSC, T_c raised to more than half way to room temperature. Data from Ref. [7], (b) Schematic phase diagram of HTSC cuprates as a function of hole doping.

forms of spectral weight at low energies are suppressed. These phenomena are associated with the opening of a pseudogap [17]. Despite a lot of effort both experimentally and theoretically to determine the nature of pseudogap, there is still no consensus on its underlying mechanism.

Neutron scattering has proven to be vital in revealing exotic and new properties of HTSC since their discovery. This is especially since the SC phase of cuprates is close to the AF insulating phase and hence one expects an interplay between magnetism and superconductivity[6]. Hence, if magnetism is at the heart of the SC mechanism in the copper oxides, a detailed understanding of the magnetic excitation spectrum is crucial. Before presenting the main results of neutron scattering experiments on HTSC, in the next section we briefly describe some aspects of neutron scattering including an introduction on the theoretical formalism that applies to magnetic neutron scattering[7].

2. Neutron scattering

Neutron scattering technique, both elastically and inelastically, has been used in many areas of condensed matter almost from its discovery about 60 years ago. The main reason for wide application of this technique is due to the unique physical properties of the neutron. Since it has no electric charge, it interacts with the nucleus via the nuclear strong force while it does not interact[8] with the electrons in a way that the electromagnetic radiation does. Since the mass of a neutron is similar to the mass of atomic nuclei, its energies and wavelengths (both thermal and cold) match the energy and wavelength scales of many condensed matter systems, it is possible that both structure and dynamics of a system be studied via neutrons[9]. Neutrons only perturb the experimental system weakly, i.e. neutrons are non-destructive. Neutrons are highly penetrating, allowing the non-destructive investigation of the interior of materials and obtaining the bulk response of the system understudy as opposed to that of the local or surface of materials. All these properties make neutron scattering a very useful technique especially in condensed matter physics.

Neutrons they could reveal the crystal structure of the system under study. This is because the diffraction pattern measured as a result of neutron interaction with materials is related to the Fourier transform of the real space structure. Since typical dimension of the nucleus of an atom is much smaller than the neutron wavelength (10^{-15} m compared to 10^{-10} m), as far as neutrons are concerned the scattering potential has no dimension and so a neutron diffraction pattern does not die away with scattering vector, i.e. it has no form factor. While the amplitude of an X-ray diffraction pattern drops rapidly away with scattering vector with a form factor which is related to the inverse of the size and distribution of the charge. In addition, since neighbouring atoms in the periodic table have very different neutron cross-sections, one is able to get contrast that would not be visible by other techniques. Also, since light elements have neutron cross-sections that are often larger than heavier elements, neutron scattering is an ideal probe to study the disorder of light elements compared to X-rays. The scattering cross-section of an atom generally varies between different isotopes of the same element enabling one to utilize isotopic substitutions to gain structural and dynamical information in detail. And finally neutron's magnetic moment is ideally suited to the study of microscopic magnetic structures and magnetic fluctuations that underpin macroscopic magnetic phenomena in materials. By coincident, the magnetic and nuclear interactions have similar cross-sections although their physical origins are completely different. This particularly makes neutrons the probe of choice in investigating the magnetic properties of materials.

In a neutron scattering experiment, the magnetic scattering function, $S_{\alpha\beta}(\mathbf{Q},\omega)$, which is the Fourier transform of the spin-spin correlation function in both time and space is directly measured. For magnetic neutron scattering, the partial differential cross-section per solid angle per unit energy is given [20] by:

6. Such close connection between SC and AF insulating phases are also observed in other exotic superconductors such as heavy fermions or some of 1D materials.

7. For a detailed theoretical treatment of the neutron scattering cross-section, see Refs. [18] for an introductory, Ref.[19] for polarized neutrons, and [20] for a more comprehensive theoretical text. Ref. [21] is an excellent detailed text on the experimental aspect of neutron scattering.

8. However, neutron can see the charge structure through changes in atomic displacements.

9. In fact, a wide range of energies may be probed by neutrons from milli-electron volt energies associated with low energy excitations of spin-waves in AF materials with small exchange coupling to a fraction of an electron volt associated for example with high energy excitations of HTSC. Similarly, since the wavelengths of neutrons is similar to atomic distances, measurements over distances from that of the wave function of the hydrogen atom to those of macromolecules are possible.

$$\frac{d^2\sigma}{d\Omega dE_f} = \frac{k_f}{k_i} N(\frac{\gamma r_0}{2})^2 \mid f(\mathrm{Q}) \mid^2 e^{-2W(\mathrm{Q})} \sum_{\alpha\beta} (\delta_{\alpha\beta} - \hat{Q}_\alpha \hat{Q}_\beta) S_{\alpha\beta}(\mathrm{Q},\omega) \,, \quad (1)$$

with the summation over Cartesian directions, $k_i(k_f)$ the incident (scattered) neutron wavevector, N the number of moments, $(\frac{\gamma r_0}{2})^2 = 72.65 \times 10^{-3}$ barn$/\mu_B^2$, $f(\mathbf{Q})$ the magnetic form factor, $\mathbf{Q}$ the momentum transfer in the scattering process, ω the energy transfer, and $e^{-2W(\mathbf{Q})}$ is the Debye-Waller factor. The $(\delta_{\alpha\beta} - \hat{Q}_\alpha \hat{Q}_\beta)$ term in the cross-section indicates that only the components of spin perpendicular to the momentum transfer, $\mathbf{Q}$, are probed by neutrons. The magnetic scattering function, $S_{\alpha\beta}(\mathbf{Q},\omega)$, is related to the imaginary part of the generalized dynamical spin susceptibility[10], $\chi''(\mathbf{Q},\omega)$, through the fluctuation-dissipation theorem [22]:

$$S_{\alpha\beta}(\mathbf{Q},\omega) = \frac{n(\omega)+1}{\pi(g\mu_B)^2} \chi''(\mathbf{Q},\omega) \,, \quad (2)$$

where $(n(\omega)+1) = \frac{1}{1-e^{-\hbar\omega/K_B T}}$ accounts for the Bose factor, g is the Lande splitting factor, and μ_B is the Bohr magneton. In an elastic experiment (where the incident and scattered neutron energies are equal), the correlations are probed at infinite time. From eq. (1), it could be seen that in this case, the scattering function will contain delta functions at the wavevectors corresponding to magnetic Bragg reflections. If the incident and scattered neutron energies are different (inelastic scattering), then the spin dynamics of the system under study are probed. Usually, the measured susceptibility is compared with the theoretical prediction based on a specific microscopic model. For example in a magnetically ordered system of localized spins, the elementary magnetic excitations are spin waves easily measured by neutrons. The energy range of magnetic spectrum that could be measured by an inelastic experiment depends on the neutron source. If the magnetic excitation occur at very high energies, for example in the case of HTSCs with the superexchange interaction ~150 meV between the nearest neighbour copper spins determining the characteristic energy of the spin fluctuations, higher energy neutrons produced by a reactor hot source[11] or by spallation[12] are required for complete characterization of the magnetic dynamics.

Neutron spectroscopy has provided unique information on the nature of magnetism in high temperature superconductors, on the interplay between magnetic fluctuations and superconductivity and on the role of the lattice dynamics. Due to the weakness of interaction of the neutron spin with electronic moments, large crystals are needed in order to obtain a sufficient signal to noise. This practical problem is more severe in the case of HTSC cuprates which are S=1/2 AF insulators when undoped. This is because the inelastic cross-section is proportional to S^2 and for S=1/2 it is even further reduced by about a factor of two due to zero-point fluctuations. In the metallic region of the HTSC phase diagram obtained by hole doping, these types of fluctuations are enhanced and the neutron signal is even weaker. Therefore, only a limited number of HTSC cuprates grown in form of large single crystals by the state-of-the-art crystal growth could be investigated by neutron spectroscopy. As a result until recently, about twenty years after the discovery of HTSC, only two families of cuprates had been investigated by magnetic neutron spectroscopy: LSCOx and YBCO6+x in details. Although LSCOx family does not possess a particularly high T_c at optimal doping (~39K) it has been extensively studied because of the relatively simplicity of its crystal structure, without bilayers and chains, and the availability of reasonable large single crystals with the downside of the presence of intrinsic disorder due to Sr doping. The YBCO6+x family has a special place among all HTSC materials. It was the first superconductor discovered with a T_c above liquid nitrogen temperature and a relatively simple synthesis route. It is available in almost the entire region of the phase diagram, easily tuned by varying the oxygen content in a quasi-continuous way. Another advantage is the possibility to grow large single crystals of YBCO6+x, which can be reversibly oxygenated. The downside is that, in YBCO6+x, the basic entities are magnetically strongly coupled CuO_2 bilayers, rather than CuO_2 monolayers which may complicate the inelastic neutron scattering experiments, due to the existence of an interplanar structure factor. In addition they possess the CuO chains that could also complicate the interpretation of the results. Due to the different crystal structures and doping mechanisms of these two cuprates families, the influence of lattice fluctuations, disorder and magnetic interlayer interactions on $\chi''(\mathbf{q},\omega)$ is still a matter of debate. The magnetic spectra of LSCOx and YBCO6+x, though similar at some level, exhibit several important

10. In the zero wavevector and zero frequency limit, the real part of the generalized susceptibility is the usual DC susceptibility which is normally measured via magnetization techniques such as VSM, SQUID etc.

11. A "hot source" consists of a block of graphite heated to a temperature much greater than room temperature of the heavy water (moderator for most of the neutrons from a reactor). The neutrons in thermal equilibrium with the hot source have a Maxwellian distribution with a characteristic temperature of 2000 K (compared to 300 K for the heavy water reactors).

12. Spallation pulsed neutron sources have an undermoderated neutron spectrum for which a relatively large fraction of the neutrons fail to reach a thermal distribution before they exit the moderator. Hence, the flux of high energy neutrons decreases only inversely with increasing energy and as a result higher energy and momentum transfers are achieved.

differences, and it is still largely unknown which features should be considered generic to the cuprates. The main neutron scattering properties of these cuprate families are reviewed below.

3. Neutron scattering results

3.1. AF insulating cuprates

In the undoped cuprates, strong interactions due to AF superexchange between electrons residing on Cu sites (Cu^{+2} is in $3d^9$ with $S=1/2$ and an electron per site) in the CuO_2 planes give rise to an AF arrangement of spins in both undoped (and lightly doped) LSCOx and YBCO6+x. The AF state is realized through a three dimensional (3D) long-range ordered transition below T_N which is controlled by the weaker coupling between planes, a consequence of the weak superexchange path between Cu^{+2} ions via the apex oxygens. The weak interplane coupling leads to an effective two dimensional (2D) behaviour. Such a transition to a long-range order AF state persists with increasing doping until a critical doping level is reached at which T_N drops to zero.

The spin structure and excitations of this AF state have been extensively studied with neutron scattering. In fact the importance and the existence of antiferromagnetism in undoped, insulating parent compounds of LBCOx was realized in 1987 soon after the initial discovery of HTSC by neutron diffraction experiments in La_2CuO_4 (LCO4) [23] which subsequently were verified by polarized neutron measurements [24]. The magnetic order manifests itself as magnetic Bragg peaks at (π, π) wavevector[13]. In LCO4, the moments align along the (1, 1, 0) direction [25]. There is a small spin anisotropy due to antisymmetric exchange [26] which leads to a small canting (~0.003 rad) of the spins out of the CuO_2 plane. In YBCO6+x, the moment direction is along the (1, 0, 0) implying a small in-plane anisotropy [27]. The value of the ordered moment, experimentally reported between 0.3-0.6 μ_B, appears to be strongly reduced from 1 μ_B corresponding to free Cu^{+2} ions with $S=1/2$ calculated with a g-factor of 2. Quantum fluctuations expected in low-dimensional antiferromagnets with small spin, covalency effects due to hybridization of the copper and oxygen atoms, and the g-factor of Cu^{+2} have been suggested to be the cause of this moment reduction [28].

The observed AF ordering in undoped cuprates could be explained by the Heisenberg Hamiltonian:

$$H = \sum_{ij} J_{\parallel} \mathbf{S}_i . \mathbf{S}_j + \sum_{ij'} J_{\perp} \mathbf{S}_i . \mathbf{S}'_j \ . \qquad (3)$$

The first term corresponds to the coupling between nearest neighbor Cu spins in the same CuO_2 plane which is the dominant interaction while the second term represents the interlayer coupling between adjacent CuO_2 layers. Compared to inplane interactions, the interlayer interaction is much weaker but it must be

13. The AF wavevector (π, π) is in units of the dimensionless 2D reciprocal lattice.

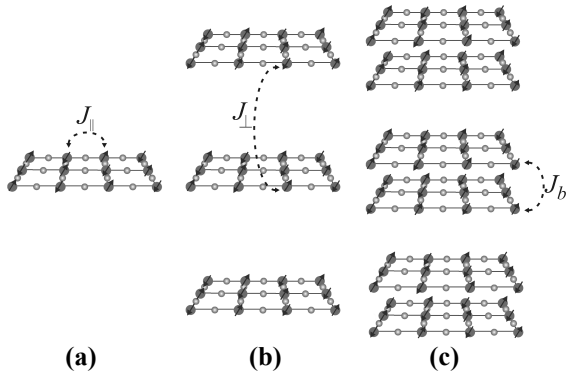

Figure 2. Schematic demonstration of (a) simple square AF case, (b) magnetic structure of LCO4, and (c) magnetic structure of bilayer YBCO6+x.

added since *real materials* have 3D structures. By neglecting the second term, eq. (3) reduces to the Hamiltonian of a (nearly) square lattice Heisenberg antiferromagnet (HAF). For HTSC materials which contain more than one CuO_2 plane per unit cell, such as YBCO6+x, an additional intrabilayer coupling, J_b, has to be considered. Figure 2 schematically demonstrate these different types of exchange interactions in HTSCs. It should also be mentioned that due to presence of the out-of-plane anisotropy α_z, the Hamiltonian is actually more complicated, i.e. the product in the first term must be substituted with ($S_i^x S_j^x + S_i^y S_j^y + \alpha_z S_i^z S_j^z$) to take this anisotropy into account [27,29].

3.1.1. AF insulating LSCOx

The magnetic properties of LCO4 and lightly doped LSCOx, could be modeled with eq. (3) assuming no interlayer coupling is present in the first approximation [30-32]. This model predicts at temperatures much less than T_N, the excitations out of the antiferromagnetically ordered ground state of eq. (3) are spin waves. The conventional spin wave theory in the classical limit (large spin) is used to calculate the dynamical susceptibility which is measured by neutron scattering experiments. The ultimate test of validity of this theory is then to compare the measured dynamical susceptibility with the prediction of this model. Due to the very large value of the exchange constant $J_{\parallel}$ of LCO4, dispersion relation in this material has a very steep slope compared to other magnetic systems that are typically studied by thermal neutron triple-axis spectroscopy. This was the main cause of failure in measuring the dispersion relation for LCO4 initially. In a reactor based thermal neutron experiment, energy transfers of only up to ~50-70 meV are easily accessible. At such energies due to a finite instrumental resolution, the two counter-dispersing spin wave modes rising from an AF reciprocal lattice point cannot be resolved in momentum space. Hence the original experiments were only able to place a lower bound on the spin wave velocity of 400 meV Å [33,34],

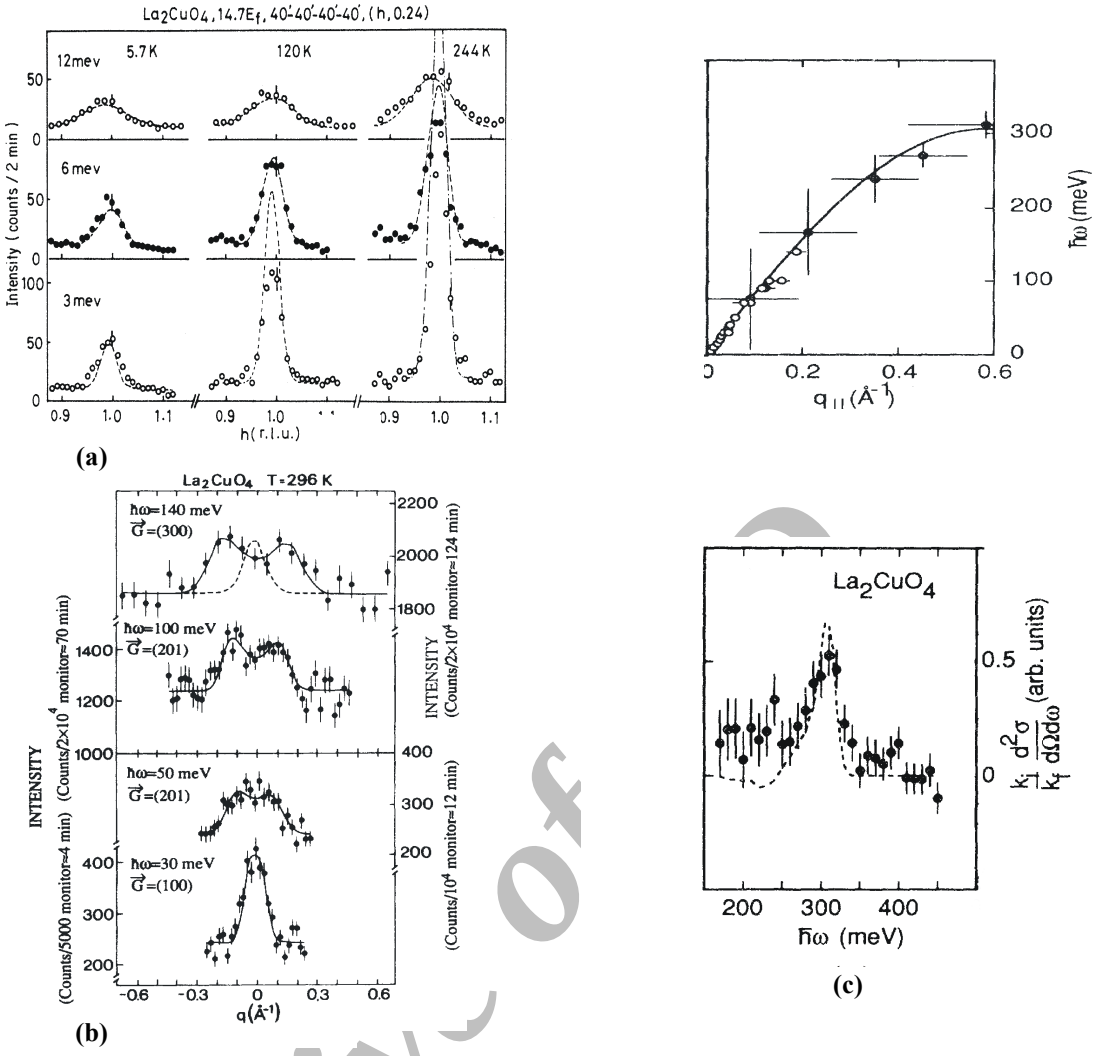

Figure 3. (a) Thermal triple-axis constant energy transfer scans through the AF zone center, (1, 0, 0), at temperatures below T_N. The dashed lines show fits to conventional spin wave theory convolved with the spectrometer resolution. Only a lower bound (650 meV-Å) on the spin wave velocity could be obtained. From Ref. [34], (b) Using higher energy neutrons available at a "hot source" at the Institute Laue-Langevin (ILL), the spin waves at higher frequencies, where the two branches emerging from (1, 0, 0) and equivalent positions are separable, were measured allowing a determination of the spin wave velocity. The dashed line in the upper scan shows the resolution limited response while the solid curves are the results of fits to a resolution convolved spin wave spectrum with a velocity of 850 meV-Å. From Ref. [36], and (c) Spallation neutron sources have sufficient undermoderated epithermal neutrons to permit measurements with incident neutron energies up to 2 eV, allowing access the energy transfer high enough to observe the zone boundary magnon mode in LCO4 (bottom) at 312 meV. The time of flight data obtained at the spallation neutron source ISIS (filled circles) combined with the triple-axis measurements shown in (a) (open circles) allowing the full dispersion relation for the spin waves be determined (top). From Ref. [37].

see figure 3(a). Later, experiments with larger energy transfers were performed using intense high energy neutron beams from both a hot source, see figure 3(b), and a spallation neutron source extending beyond the thermal and hot range, see figure 3(c). In these experiments, the energy transfers were large enough to separate the spin wave modes and the spin wave velocity was unambiguously determined from the location of resolved spin wave peaks in constant energy scans [35-37]. These measurements result in a exchange constant, $J_{\parallel}^{*}=153\pm4$ meV (corresponding to a $J_{\parallel}$ of 135 meV appearing in eq. 3 based on a renormalization of the energy scale of the spin waves) as well as an upper bound on the next nearest neighbor exchange constant of 9 meV. Later neutron scattering experiments of the spin waves in LCO4 over the full Brillouin zone were placed on an absolute scale [28,38] and hence made it possible to determin the quantum renormalization of the magnetic response. Such studies have provided a quantitative verification of the applicability of renormalized spin wave theory and a determination of the parameters of the magnetic Hamiltonian (eq. 3) that describe this material.

An interesting question is whether the spin dynamics of LCO4 are changed by the Neel transition [39-44]. Neutron scattering studies show that the spin dynamics

of LCO4 are not considerably affected by this transition as only a small 3.6 ± 2.9 meV damping at 320 K [36] is observed. This indicates that very long range 2D correlations exist in the paramagnetic state since the 3D ordering is driven by the weak interlayer coupling with small effect on the intralayer dynamics for energies comparable to $J_{\|}^{*}$. At low (<5 meV) energies the transition to the paramagnetic state results in an additional quasielastic contribution to the cross-section due to spin wave interactions with a width of 1.5 ± 0.4 meV in good agreement with both theoretical expectations [39] and numerical simulations [40].

LCO4 can be doped by replacing La with Sr or Ba which introduce holes in the CuO_2 planes. Increasing doping level eventually leads to an insulator-metal transition and a SC ground state at a critical doping level. Doping not only changes the charge transport but also the low energy magnetic properties. The Neel temperature is suppressed strongly by increasing doping due to the frustration associated with a hole that substitutes a ferromagnetic bond for an AF one. For doping level greater than x~0.015 no longer a long range ordered AF state exists at low temperatures [45]. Upon further doping, carrier localization below 100 K and 2D spin-glass freezing characterize [45] samples with doping 0.015<x<0.05. For these doping levels although a long-range AF ordering does not occur, strong AF correlations are still present (evidenced by peaks in the energy integrated neutron cross-sections at the same position, (π, π) as in undoped LCO4 [42]). This behaviour is similar to that observed for the paramagnetic state of LCO4 but the inverse correlation length saturates at a doping dependent value on cooling. The increase in inverse correlation length with increasing temperature follows the same renormalized classical form as the undoped material. This suggests the growth of correlations is limited by the mean spacing between impurities. The study of the magnetic dynamics also indicates a shorter characteristic length scale associated with lightly doped LCO4 as constant energy scans remain centered on the (π, π) position with a width that is always broader than the instrumental resolution [37] by increasing transferred energy. The energy dependence of the local (**Q**-integrated) susceptibility is temperature dependent at low energies:

$$\chi''_0(\omega) = \chi''_0 \, tan^{-1}(\frac{\omega}{\Gamma}) \qquad (4)$$

Above 50 K, the crossover from localized to conducting transport behaviour, the lifetime $\Gamma \sim T$ impling the spin dynamics exhibit ω/T scaling [42]. This type of scaling is consistent with the marginal Fermi liquid theory used to explain other anomalous normal state properties of the HTSC cuprates [46].

3.1.2. AF insulating YBCOx

Among all HTSC materials, YBCO6+x system is perhaps the most extensively studied by different experimental techniques including neutron scattering

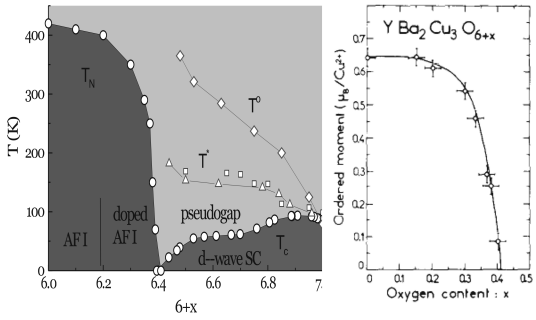

(a) **(b)**

Figure 4. (a) A representative phase diagram for YBCO6+x. From Refs. [53,47], (b) The ordered moment doping dependence. From [47].

technique [27,47-50]. The antiferromagnetically ordered parent compound is YBCO6 and superconductivity occurs as a result of introducing holes into the CuO_2 planes by adding additional oxygens to the CuO chains. At low oxygen concentration ($x < 0.4$), the YBCO6+x samples have a tetragonal crystal structure. These samples are insulators and possess a long range ordered AF ground state below T_N. The samples with $0.0 < x < 0.2$ are undoped, while for $0.2 < x < 0.4$ samples are doped AF insulators. Increasing dopingl eventually destroys AF ordered state completely (for $x_c \approx 0.40$) [47]. A rough[14] phase diagram is presented in figure 4(a) which shows the suppression of T_N and the onset of superconductivity which occurs for x~0.45.

YBCO6 is usually classified [27] as an ionic compound with well defined valence states $Y^{+3}Ba^{+2}Cu(1)^{+1}Cu(2)_2^{+2}O_6^{-2}$, where Cu(1) ions reside on the CuO chain layers while Cu(2) ions are located on CuO_2 planes. In this material the chain Cu ions are monovalent with a nonmagnetic (spin=0) $3d^{10}$ electronic configuration and as a result do not participate to the magnetic ordering of the system. The magnetic ordering involves only the bivalent planar Cu ions. Below T_N, an AF ordering of planar Cu spins takes place with the spins laying in CuO_2 planes [52] with the spin arrangement described by a 2D wavevector **Q**=(π, π). From the absence of intensity at $l = 0$ (l is the Miller index corresponding to the c-axis), it is established firstly the AF nature of intrabilayer couplings and secondly the absence of sizable contribution arising from chain Cu sites. The obtained magnetic structure also exhibits AF interbilayer couplings. Assuming an anisotropic form factor a magnetic moment of 0.52 μ_B is found [54,55] at low temperatures[15]. Upon increasing temperature, the magnetic moment decreases [47] continuously until it vanishes at 410 K. A similar magnetic ordering is observed [47] for samples with oxygen contents up to

14. Recent advances in crystal growth have indicated that the critical oxygen doping is less than 6.4, see Ref. [51].

15. Again this is much smaller than the mean field prediction of $g\mu_B S$=1.06μ_B. This reduction is explained [54,55] by both quantum and covalence effects.

6.15-6.20 with a weak change in both T_N and magnetic moment. This could be understood by considering the fact that at low concentrations ($0.0 < x < 0.15$-0.20) only isolated and randomly oriented Cu^{+2}-O^{-2}-Cu^{+2} units are created in the chain layer which maintain the tetragonal symmetry. This only changes two monovalent Cu ions into bivalent ones and hence does not induce any charge transfer to the planes. Thus pure AF state is retained. Further addition of oxygen ions ($0.2 < x < 0.40$) to the system leads to longer and longer randomly oriented chain segments. This addition of oxygen ions, while maintaining the tetragonal symmetry, now has a much stronger effect on AF ordering (see figure 4(a) and (b)).

Inelastic neutron scattering experiments have shown [27,29] that the spin dynamics of bilayers in AF YBCO6+x is well accounted for by the same AF Hamiltonian as LSCOx (eq. 3) now with three anisotropic exchange interactions: the in-plane nearest neighbor intralayer superexchange coupling ($J_{\parallel}^{*} \approx 100$-$120$ meV), the intrabilayer superexchange coupling ($J_b \approx 0.02$-$0.1\, J_{\parallel}$) and the interbilayer superexchange coupling ($J' \approx 2$-$2.5\times10^{-4}\, J_{\parallel}$, $\alpha_z \sim 0.8$-3×10^{-3}). The main difference between LSCOx and YBCO6+x has its origin in one of the distinguishing structural features of YBCO6+x, the CuO_2 bilayers. The close spacing of the CuO_2 planes in YBCO6+x structure in a bilayer (3.2 Å) gives rise to a non-zero intrabilayer coupling. The presence of the intrabilayer coupling leads [29] to two branches in the spin wave dispersion which differ according to whether spins in adjacent layers rotate in the same ("acoustic") or different ("optic") directions. The $\sin^2$ and $\cos^2$ modulations along c-axis can be used to distinguish between the two modes (for more details see Ref. [27,29]). Due to the relatively large value of in-plane AF coupling constant, initial studies of YBCO6+x for AF compositions were not able to probe high enough frequencies to resolve the acoustic spin wave or observe the optic mode gap. Most of neutron scattering experiments were done on the acoustic branch. More recent measurements [56] have revealed the existence of an optic gap (given by $\hbar\omega = 2\sqrt{J_{\perp} J_{\parallel}}$ at the magnetic zone center) at much higher energies around 70 meV. Figure 5(a) shows the experimental data of both acoustic and optic modes in YBCO6.15. In case one considers as well interlayer coupling and out-of-plane anisotropy, additional lifting of the degeneracy at low energies can be observed (for a more detailed treatment of the spin wave theory, including additional, smaller, terms in the Hamiltonian see Ref. [29]). The quantum renormalization of the spin wave amplitude determined from neutron scattering measurements at spallation sources is in agreement with the LCO4 data [38] and the $1/S$ expansion [32]. The optic mode, corresponding to out of phase motion of spins in adjacent layers of a bilayer, has also been observed by both reactor based hot source triple-axis scattering [56] and spallation source time-of-flight [58] techniques. Figure 5(a) shows the energy dependence of the local susceptibility for values of c-axis momentum transfer chosen to probe the acoustic and optic mode response. The observed gap energy of 74 ± 5 meV implies $J_{\perp}^{*} = 11 \pm 2$ meV close to band theory calculations [59].

Despite the similar $J_{\parallel}$, the Neel temperatures in insulating LCO4 and YBCO6 are rather different: $T_N \sim 325$ K in LCO4 [42] and $T_N \sim 515$ K in YBCO6 [29]. This is because a purely 2D Heisenberg system does not order at $T > 0$, and the interlayer interactions that ultimately drive the transition to long range order are rather different in the two systems, being almost frustrated in LCO4 but unfrustrated in YBCO6. More importantly, the spin system of YBCO6 consists of weakly coupled bilayer units with strong intra-unit exchange interactions ($J_{\perp} \sim 10$ meV [56]) whereas the unit in LCO4 consists of only a single layer. These strong intrabilayer interactions are manifested throughout the phase diagram of YBCO6+x, and they are an important possible origin of differences between the two systems. In addition, the absence, or near absence, of disorder in YBCO6+x contrasts sharply with the situation in LSCOx where disorder due to Sr acceptors is always present.

3.2. Superconducting cuprates

One stark contrast between simple metals and HTSC materials is the presence of strong AF correlations (a result of enhanced electronic interactions) in both their SC and normal states with their normal state as anomalous as their SC state. For a simple standard paramagnetic metal (such as Al, Cu, etc) with weak electronic interactions, the spin susceptibility exhibit very weak momentum dependence and extends up to energies defined by the bandwidth ($d\varepsilon \sim$eV) of the metal with its amplitude proportional to $1/d\varepsilon \sim 1\ \mu_B^2/$eV [22]. For such materials the electronic spin fluctuations are then usually too weak to be detected in inelastic neutron experiments. In HTSCs, quite the opposite, magnetic correlations persist well above T_c, centered around the AF wave vector, (π, π), in YBCO6+x [60] and LSCOx [61] with an amplitude of several 100 $\mu_B^2/$eV. This behaviour is drastically different from what is expected for any conventional superconductor in both normal and SC states and suggests the importance of antiferromagnetism in the microscopic description of the HTSC cuprates. Although signs of the magnetism persist far into the SC region of the phase diagram, while undoped AF compounds have well-defined excitations (as described above), doped materials behave in a very complicated manner with dramatic changes on the energy, momentum dependence of the spin excitations induced by doping. Neutron scattering experiments on SC cuprates indicate the presence of local order with short length scales. This local magnetic order appears as

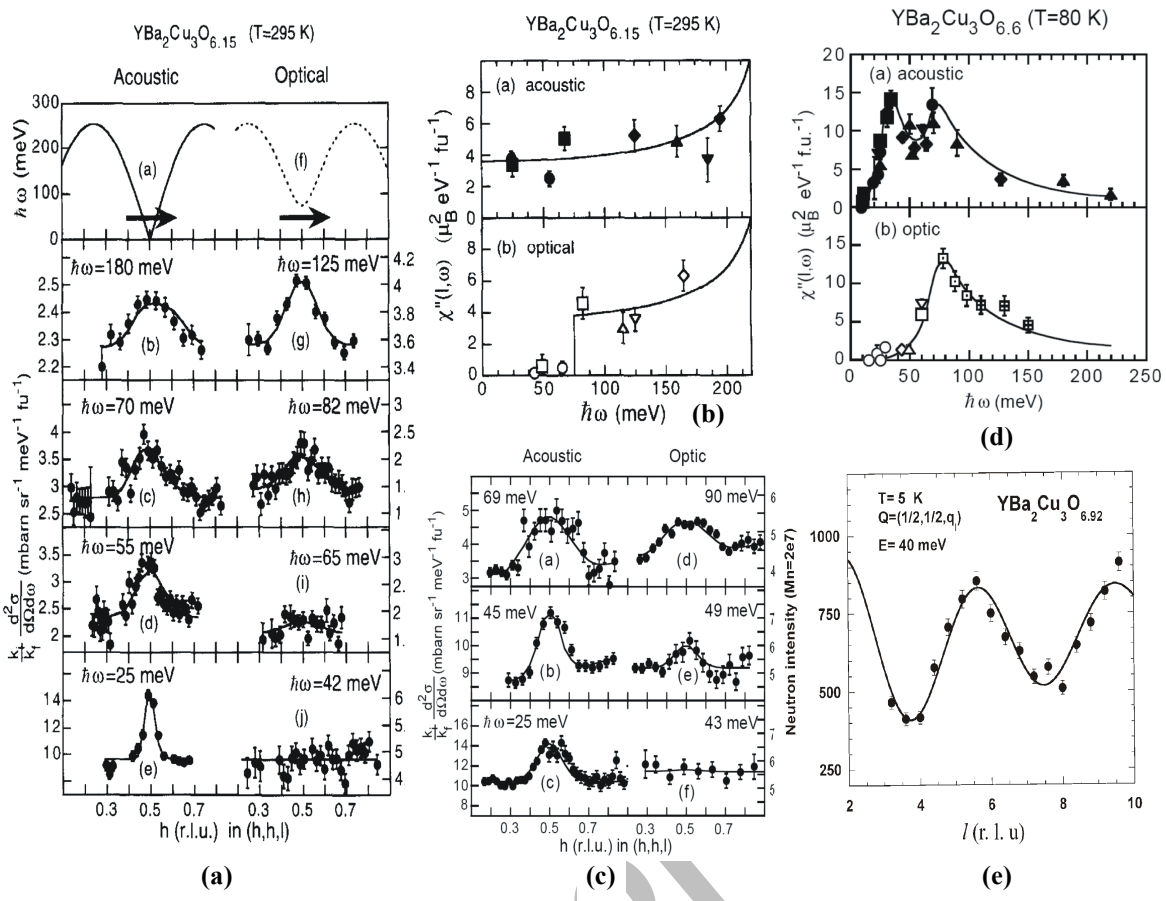

Figure 5. Constant energy scans showing magnetic scattering from YBCO6.15 (a) and YBCO6.6 (c) for wavevectors Q=(*h*,*h*,*l*). In the left panel, *l* was chosen to emphasize acoustic modes while for the right panel, it was chosen to emphasize optic modes. The onset of scattering at the optic position is about 74 meV. (b) Energy dependence of the local susceptibility of YBCO6.15 (b) and YBCO6.6 (d) obtained by integrating over spin wave peaks and correcting for the Cu^{+2} magnetic form factor, Bose factor, and instrumental resolution for the (top) acoustic and (bottom) optic spin wave modes. The optic mode gap of 74 meV implies an inter-planar coupling of ~ 11 meV. Solid lines correspond to fits to spin wave theory. All experiments were performed using the ISIS pulsed spallation source. Note the large spectral shift from insulator YBCO6.15 to conductor in YBCO6.6. From Ref. [58], (e) *l*-scan at 40 meV in YBCO6.92 displaying a modulation typical of odd excitations. From Ref. [60].

broad incommensurate peaks around the (π, π) Bragg peak position of the undoped antiferromagnet, but displaced by an amount that increases with hole doping [62-65]. Even when there is no longer static order, these peaks persist as excitations seen by inelastic neutron scattering. Also, there is a drastic change as one enters the SC state via a strong renormalization of the spectral weight distribution whose two most salient features are opening of a spin-gap manifested by the observation, in the vicinity of the (π, π) point, of a depletion of the spectral weight at low-energies observed both in LSCOx and YBCO6+x compounds, and emergence of a resonance at (π, π) position for superconductors having the highest T_c's (YBCO6+x and Bi-based materials) where a strong build up of intensity is observed at energies larger than the spin-gap energy. Below we consider these properties in more details.

3.2.1. Superconducting LSCOx

In LSCOx, the low energy spin fluctuations qualitatively change for doping larger than x_C. Early studies showed that with doping, the long-range Neel order gives way to short-range order with a progressively shorter correlation length so that at optimal doping the static spin correlation length is no more than two or three lattice spacing. An enhanced spin scattering is found [63] at low energies centered at the incommensurate positions, δ, along (π, 0) and (0, π) directions[16]. The enhanced scattering observed at the incommensurate positions is considered to be related to the formation of stripes[17]. Figure 6(a,b,c) shows some examples of momentum and energy dependence of incommensurate response with different types of doping. The intensity of the incommensurate scattering rapidly decreases as the temperature is increased to 100 K. The peaks are quite

16. This is in a notation appropriate for a square lattice where the magnetic instability in the undoped case occurs at (π, π).

17. The formation of stripes is further evidenced by a recent neutron scattering study of the bond-stretching phonon mode [66].

sharp in momentum space indicating that on time scales comparable to the inverse of the frequencies probed (1-15 meV) the correlation lenghts are larger than the mean spacing between impurities (the limiting factor for static correlations in lightly doped LSCOx).

It is found [62,67-69] that δ increases systematically with doping (proportional to x) shown in figure 6(d). This doping dependence is similar to that of T_c. The presence of incommensurate excitations however is not limited to the superconducting samples as some samples with no SC transition exhibit an incommensurate response. More interesting as seen in figure 6(d) is the sudden change from commensurate to incommensurate fluctuations at x~0.06 which incidentally coincide with the metal-insulator transition. In addition, δ saturates for doping larger than optimal doping (x=0.14-0.17). Similar studies for overdoped samples have not been possible since homogeneous single crystals with $x > 0.2$ are not available due to difficulties in crystal growth.

The dependence of the incommensurate response on energy has been studied [70], see figure 6(c) for LSCO0.14 at 35 K (just above T_c). As seen at low energies the incommensurate peaks are well defined but broaden with increasing energy, so that the data at 15 meV do not displays well resolved incommensurate features any longer. This energy-momentum dependence is somewhat similar to that observed in Cr and Cr alloys above the SDW transition [71]. The lines in figure 6(c) are the results of a fit to a functional form [72] to describe Cr but modified to include the 2D nature of the incommensurate magnetism in LSCOx. Based on further experiments [61] with better signal to noise, it is shown that this simple mean field model cannot simultaneously describe the momentum and energy dependence of the spin fluctuation in the normal state of LSCO0.14. However this model describes the general behaviour of the low energy peaks merging into a broad, flat topped, commensurate response at higher energies which also occur in the Cr systems. At energies higher than ~ 25 meV the incommensurate character of the magnetic response disappears [69]. Although it should be mentioned that due to the presence of optical phonons this interesting regime where incommensurate-commensurate cross-over happens has not been fully studied.

The similarity of the wavevector of the dynamic incommensurate structure observed in LSCOx to the static charge and spin ordering in compounds nearby in phase diagram suggests stripe formation may be the driving mechanism. This is used as an explanation for both the anomalous normal state properties and the underlying origin of superconductivity [73] in cuprates.

The characteristic incommensurate fluctuations of the metallic and SC LSCOx is a low energy feature which eventually merges into a broad commensurate response above ~ 20 meV, similar to lightly doped insulating samples. Since the magnetic response of insulating LSCOx extends over energies up to 320 meV, a similar energy scale might also be expected for SC compositions. Figure 7(a) shows a comparison of the energy dependence of the response in LCO4 and LSCO0.14 with the intensity units normalized to allow a direct comparison. The schematic diagrams at the top of this figure show how doping modifies the spectrum. The magnetic excitations stemming from the commensurate AF position are broader in momentum, indicating shorter characteristic length scale, and fall off more rapidly at higher energies. The local susceptibility, obtained by integrating the response in momentum space is shown in figure 7(b) for the same two samples. As seen the doped compound has spectral weight over the same large rangeof energies as the AF insulator however a major redistribution of spectral weight from high energy to a peak in the response at ~ 20-30 meV has occured.

In general SC transition should have a dramatic effect on the spin response of a system. For LSCOx the low energy incommensurate peaks in LSCOx could be arising from transitions across the Fermi surface which a quasiparticle moves from an occupied to an unoccupied state while flipping its spin leading to the particle-hole excitation to acquire a gap of 2Δ. In fact, consistent with this picture, neutron scattering experiments on LSCOx indicate that the low energy spin fluctuations are suppressed below T_c. However, the effects of SC transition, summarized in figure 7(c), appear to be more complex [64] and the observed behavior cannot be fully explained based on a simple picture of non-interacting Fermi surface particle-hole analogy. The most significant signature of such a difference is the incomplete suppression of the low energy excitations below T_c (see 6.1 meV data in figure 7(c)). This is quite different from what is expected for a clean conventional superconductor where no particle-hole excitations exists for energies less than 2Δ. Neutron scattering experiments have indicated that the low energy response is sample dependent [75]. This suggests an impurity induced low energy response in the SC state might be responsible for incomplete suppression of excitations below T_c. One should also remember that for a d-wave superconductor, there are non-zero low energy response associated with the d-wave symmetry of the gap. However a modification of the wavevector dependence of the low energy response is predicted due to a d-wave order parameter [76] which has not been observed [77]. In addition, the theory cannot explain the fact that the enhancement below T_c for energies above 7 meV occurs only for a very narrow region of $\mathbf{Q}$ near the incommensurate peak. All of this is an indication that there is still a long way to the complete understanding of the spin excitations in HTSC LSCOx and their relationship with superconductivity.

3.2.2. Superconducting YBCO6+x

For SC YBCO6+x, similar to LSCOx, strong magnetic fluctuations are observed [27,60] in the SC state. The magnetic scattering is peaked in an area around the AF wavevector (π, π) with a correlation length that decreases with increasing x, see figure 8.

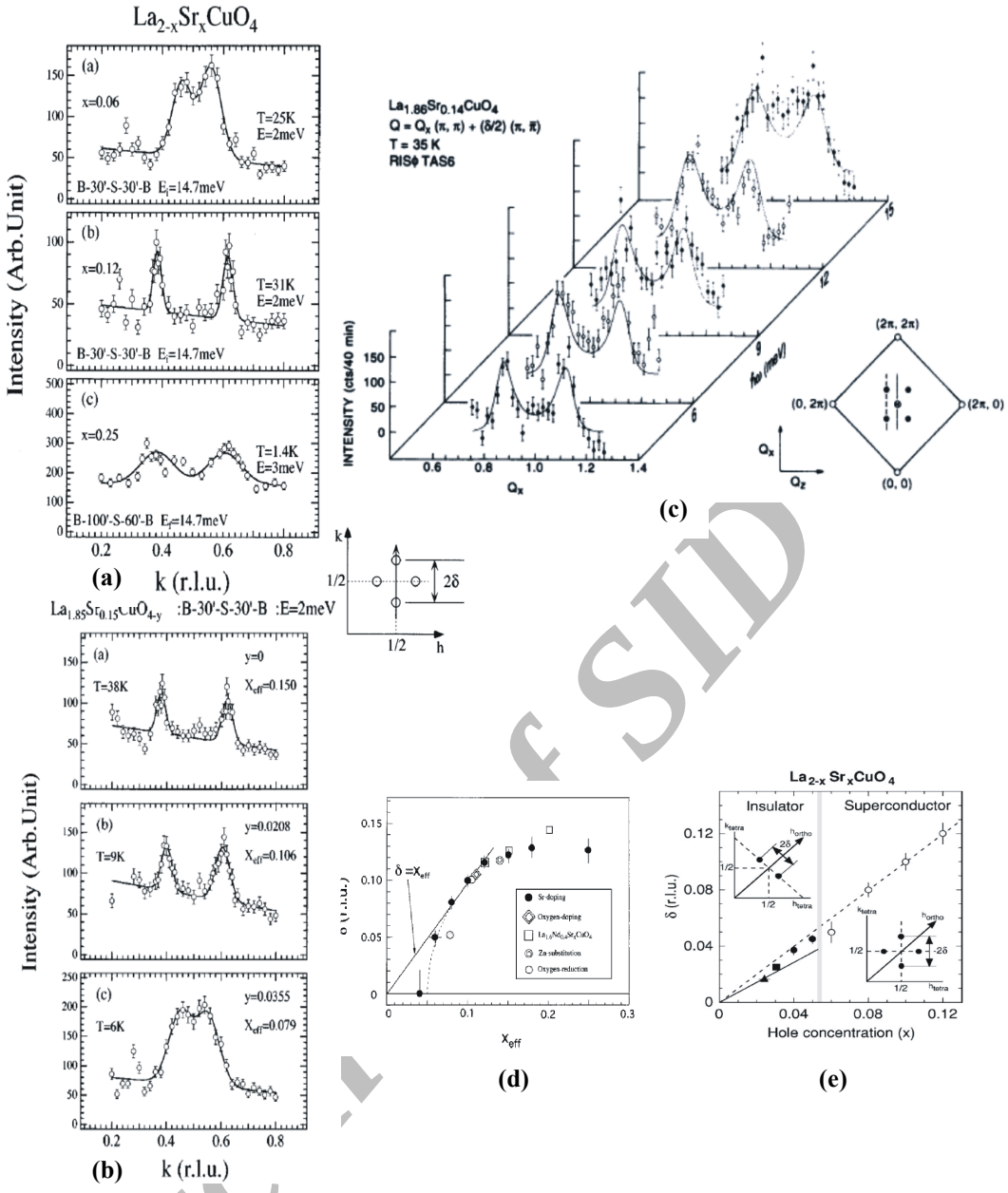

Figure 6. (a) Inelastic thermal neutron scattering spectra of LSCO from q scans across the two peaks shown by open circles in the inset; (top) x=0.06 at 2 meV, (middle) x=0.12 at 2 meV, and (bottom) x=0.25 at 3 meV. The solid lines are the results of least squares fitting using two Gaussians plus a flat background. The incommensurability δ is defined as half of the peak splitting between the two peaks at (1/2,1/2±δ,0) indexed in the tetragonal reciprocal plane (h,k,0). The position (1/2,1/2,0) corresponds to an AF Bragg peak position in the long-range-ordered AF phase. From Ref. [67], (b) Inelastic neutron-scattering spectra at 2 meV taken from (top) the SC sample with x=0.15, and the deoxygenated nonsuperconducting crystal with x=0.15 with the effective doping of x_{eff}=0.106 (middle) and (bottom) with x_{eff}=0.079. The δ's for the deoxygenated samples are shown in panel (d) as a function of x_{eff}, (c) Energy and momentum dependence of the incommensurate spin fluctuations in the normal state of LSCO0.14. The inset in the lower left shows the scan trajectory in the 2D square lattice momentum space (dashed line). The low frequency incommensurate response broadens with increasing energy, merging into a broad commensurate feature as the energy is increased beyond~15 meV. From Ref. [64], (d) Incommensurability, δ, of the spin fluctuations in LSCO and related systems as a function of the effective doping level. The magnitude of the incommensuration scales in roughly the same way as T_c with doping. From Ref. [67]. (e) Plot of the incommensurability δ vs hole concentration x. In the SC samples, the open circles denote the position of the fluctuating spin-density wave observed by neutron scattering. In the insulator the SDW becomes static at low temperatures and its orientation is rotated by 45°. The dashed line δ =x is the prediction of the stripe model, which assumes a fixed density of holes along the stripe. From Ref. [70].

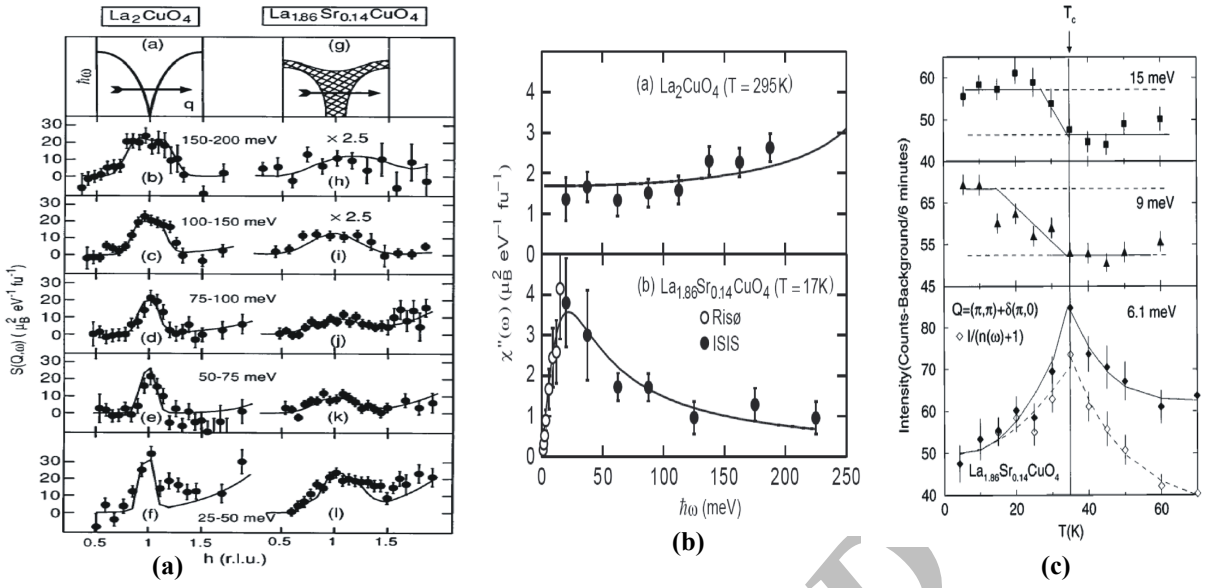

Figure 7. (a) Magnetic scattering from LCO4 (left panel) and from LSCO0.14 (right panel) between 25 and 200 meV. The overall energy scale in the two systems is comparable but the magnetic peak is broader in the superconductor and the intensity is suppressed at higher frequencies. From Ref. [30,38], (b) Local susceptibility derived from data such as that in (a) (closed circles) and from reactor-based measurements [61]. Note huge redistribution of spectral weight caused by doping. From [30], (c) Temperature dependence of the incommensurate magnetic response in LSCO0.14 for different energy transfers. For energies below 7 meV the spin fluctuations are suppressed while at higher energies they are enhanced. From Ref. [74].

Both a sharpening of the incommensurate peaks and an removal of the lowest energy fluctuations are observed upon SC transition similar to optimally doped LSCO0.14 [74].

A unique neutron scattering property of YBCO6+x is the presence of a resonance peak (figure 9(a)) which is not observed for LSCOx cuprates. The initial measurements of the low energy spin fluctuations in YBCO6+x for samples with oxygen content larger than x~0.5 discovered the presence of a peak (see the neutron resonance section below for details), centered at the commensurate (π, π) position and much broader in momentum than in insulating YBCO6+x [47,57,78,79]. The doping dependence of this commensurate response is shown in figure 9(b) for SC YBCO6+x. Such measurements at higher doping are increasing more difficult due to a shift in the characteristic energy of the scattering and overall decrease in intensity as the peak smears out in momentum space. It is worth emphasizing the fact that the magnetic response is observable only in a surprisingly small energy range and falls down rapidly above 60 meV ($\approx J_{\parallel}/2$). With increasing doping, the low energy part is more and more depressed, due to the opening of a gap E_g (the so-called spin-gap), whereas the magnetic scattering vanishes more and more rapidly at high energy. The gap increases continuously with x, with typical values E_g=4.5 meV for x~0.5 ($T_c \approx 47$ K) and 28 meV for x~0.92 ($T_c \approx 91$ K) [60]. In addition, with increasing doping, the overall energy integrated intensity[18] decreases. This contribution dominates in the weakly doped regime, whereas it is strongly reduced in the overdoped regime, for which almost only a narrow resonance peak is observed. The weakness of the localized contribution in the overdoped regime may be the cause of the different behaviors observed in the underdoped and overdoped regimes.

Figure 5(d) shows the local (**Q**-integrated) susceptibility up to 200 meV for x=0.6. Similar results have been obtained for x=0.5 [60]. The most dramatic feature in figure 5(d) is the significant difference in overall energy dependence and the absolute intensity compared to that of figure 5(b) for the spin waves in a sample with x=0.15. There is a shift in spectral weight to lower frequencies in the metallic sample. Despite this different behaviour, there are similarities between the insulating and superconducting materials such as similar c-axis dependence for spin excitations, see figure 5(e). As was the case for the spin waves, the low energy response is the acoustic mode, peaked at the c-axis wavevector that corresponds to a π phase shift within a bilayer [28,56].

For $6.6 < x < 7$, while the optic mode is nearly unchanged (apart from a renormalization factor), the excitation associated with the acoustic mode appear broadened[19] in wavevector along with a decrease in the

18. Here this integration is for energies less than ~ 50 meV and hence does not indicate any sum rule but just display the doping dependence of the spectral weight of the measured AF dynamical correlations within an arbitrary energy range.

19. This could be understood [27] by considering the fact that every hole transferred to the plane creates a defect in the network of AF bonds of the square lattice. An orientational disorder, a magnetic polaron, is created to accommodate this defect. The in-plane correlation length is directly controlled by the average polaron-polaron distance (number of holes per Cu/a^2). Hence for x=0.37, one obtains n_h=0.015.

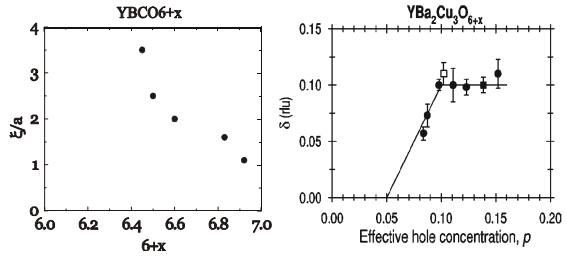

Figure 8. (a) In-plane correlation length vs. oxygen content. From Ref. [27], (b) The incommensurability δ as a function of effective hole concentration, p, calculated from $T_c/T_{max}=1-82.6(p-0.16)^2$ with $T_{c,max}=94$ K for YBCO6+x materials. From Ref. [80,81].

intensity [27]. This broadening is associated with the presence of a short range magnetic correlation. From the linewidth of the peaks observed, the correlation length, ξ, is found to decrease by increasing the oxygen content [27] (see figure 8(a)). This is an indication that the intralayer couplings are preserved even at these doping levels. Recent high resolution neutron scattering experiments on high quality crystals have shown [80,81] that the broadening of the AF peak in doped YBCO6+x is in fact partially due to presence of incommensurate peaks around the AF wavevector. Such experimental results invoked considerable discussion on the inhomogeneous states in cuprates [82]. The incommensurability in YBCO6+x increases with T_c for low oxygen doping and saturates to $\delta \sim 0.1$ for $x > 0.6$ (see figure 8(b)). In addition, the incommensurability decreases with increasing energy close to the resonance [80,81]. By analogy to LSCOx [83], one might be tempted to ascribed the presence of the incommensurate fluctuations in YBCO6+x to an underlying charge/spin ordering associated with the stripes.

Since initial measurements of the inelastic magnetic response of SC compositions of YBCO6+x found only a broad commensurate peak at low energies (in contrast to the incommensurate response found in LSCOx), it was suggested that differences in the Fermi surface geometry of the two compounds could be responsible [84]. But with recent measurements showing [80,81] for a sample with x=0.6 a clear incommensurate response, see figure 9(a) with the locations of the peaks same as for equivalently hole doped LSCO0.1 [81], it seems that the low energy incommensuarte excitations are a universal feature of HTSC materials. To fully resolve how the incommensuration depends on oxygen content further detailed measurements are required.

In a SC mechanism based on magnetism, the effective interaction would be directly proportional to the spin susceptibility measured in the normal state. The determination of the neutron spectrum above T_c is then of great importance. The evolution of inelastic spectrum with doping in the normal state of YBCO6+x is shown in figure 9(c). For both underdoped and optimally doped samples, a maximum in the dynamical susceptibility is observed [60] at a finite energy (ω_m). In the limited range of $T>T^*$ (pseudogap temperature, see below) and energies less than ω_m, the dynamical susceptibility can be fitted with a scaling relation similar to eq. (4).

Interestingly, similar to the SC state, a drastic decreasing of the AF susceptibility amplitude is found as a function of doping in the normal state. Although in the SC state the magnetic response is more and more dominated by the resonant part upon doping, the normal state of the overdoped regime is characterized by a very weak magnitude of the magnetic signal, in sharp contrast to the underdoped case. This may be an explanation for the absence of a pseudogap and for the nearly Fermi liquid behavior observed in the overdoped regime. At first glance, it might also suggests that AF fluctuations cannot be important for the HTSC mechanism as the magnetic fluctuations seem to vanish for samples where T_c is almost as large as the maximum T_c. However, considering the fact the Q width of the magnetic scattering increases by increasing doping [85] leading to the total spin susceptibility (i.e. AF fluctuations) that is still large enough to result in a sizeable T_c. Also the doping dependence of the spectral weight has a similar behaviour as the pseudogap indicating that the existence of strong AF fluctuations is directly related to the presence of pseudogap. The doping dependence of the magnetic response of YBCO6+x potentially could be understood based on a balance between the localized (associated with Cu spins) and the itinerant (associated with hole motion) contributions. Despite a lot of effort [86,76], at present a theoretical treatment of such a dual coupled system that could predict the presence of spin-gap, resonance, pseudogap and their temperature and doping dependence is not available yet.

3.3. Neutron resonance

In the past decade, neutron scattering experiments on YBCO6+x have converged on a common property of the spin excitations in this material, namely the existence of the so-called neutron resonance which is also observed in Bi-based cuprates. This resonance has dominated much of the interest in inelastic neutron scattering from YBCO6+x both experimentally and theoretically[20]. Especially because it was observed that the intensity at resonance energy increases below SC transition. However, one cannot rule out that resonance is a consequence of SC as opposed to the cause of it. For optimally doped YBCO6+x, as one increases the energy, the incommensurate peaks condense [48-50] into a strong narrow peak a well defined energy $E_r=40$ meV, defining the "resonance peak" (see figure 9 for an example). This peak was first observed [57] as a sharp, intense peak at (π,π) that appeared below T_c in optimally doped YBCO6+x. As the detailed energy dependence is obscured by the presence of an accidentally degenerate

20. While the resonance is an interesting and prominent phenomenon in the excitation spectrum of the cuprates, its spectral weight is only, of order 2% of the total spin moment sum rule for optimal doping (increasing somewhat for underdoped materials). Therefore, one needs to be cautions on the amount of emphasis put on this feature, see Ref. [87].

phonon in energy and momentum, polarized neutron scattering experiments were performed on samples with x=0.93 [49] to separate the magnetic scattering from this phonon confirming the magnetic origin of the resonance peak.

The position of the resonance peak is strongly dependent on the doping level [48-50] evolving from about 5-7 meV for YBCO6.4, 34 meV for YBCO6.6 and up to 41 meV for optimally doped samples whereas simultaneously the spectral width decreases. The overall variation with T_c is summarized in figure 9(d). As seen in this figure, the resonance following $T_c(x)$ with doping. This suggests that resonance might be the soft mode of superconductivity as a function of doping and that it is closely connected with superconductivity and itinerant holes.

The temperature dependence of the resonance peak is studied in samples with different doping level as well. In highly doped YBCO6+x, the resonance peak appears exactly at T_c and becomes less and less important as x decreases from 1 to x_C [48-50]. The fact that the resonance peak is more apparent below T_c in optimally doped materials could be associated with the fact that below T_c the SC gap increases the density of states at this energy. Also, the resonance peak which exists exclusively below T_c for highly doped materials, appears above T_c for underdoped compounds with $x < 0.8$ [80,81]. The general trend of the normal state response shown in figure 9 indicates a gradual elimination of the intensity at (π, π) in the normal state as the oxygen content is increased beyond optimal doping (x~0.93). For underdoped materials although the growth in the intensity at the resonance energy begins well above T_c, there is a rapid increase, and an associated reduction in energy width, which occurs just below T_c. The size of the peak in the normal state is reduced as the oxygen content is increased and the temperature at which it becomes apparent is also reduced. This onset temperature appears to follow the pseudogap seen by NMR [80,81].

There have been intense theoretical studies to explain the presence of resonance peak. Many theoretical models including a SC coherence effect which occurs in the framework of an itinerant electron picture [88], a collective mode associated with a multicomponent, SO(5) order parameter [89], and a spin-triplet exciton bound [90] have been suggested. However, for most of these models, the existence of the resonance above T_c is a challenge. It is also suggested [27] that there is a close connection between the resonance and the SC gap. Although it cannot be a very trivial relationship since experimentally E_r remains constant whereas the SC (not the pseudogap) gap should vanish at T_c. Further support of the triplet exciton idea comes from the observation that incommensurate branches extend below the resonance energy [93]. This behavior is predicted by random-phase-approximation-type theories [94] in that the gap in the particle-hole continuum extends over a region near (π, π), where the resonance can be formed.

Since the first observation of the resonance peak in optimally doped YBCO6+x, this peak has also been long sought for the LSCOx family. However, it appears that this system does not exhibit the resonance peak. Since YBCO6+x contains CuO_2 bilayers compared to single layers in LSCOx, one could assume the resonance peak is a characteristic feature of bilayer cuprates. However, the observation of a resonance peak at (π, π) at E_r=47 meV in single layer $Tl_2Ba_2CuO_y$ [95] indicates that the bilayer structure is not a prerequisite for the occurrence of the resonance peak. Also contrary to LSCOx, for LBCOx in addition to a charge-ordered phase, a dominant feature is observed at (π, π), which is the first report of such a resonance in La-based cuprates [96]. The resonance in LBCOx is observed in the normal (charge-ordered) state displaying very similar features to YBCO6.6 SC state. The absence of a resonance peak in LSCOx may be explained by the position of the resonance mode with respect to the particle-hole continuum in that if the decay into particle-hole pairs is fast, the magnetic modes may be overdamped so that they are not seen in experiment as prominent peaks [97]. Another important factor that one has to consider in comparing YBCO6+x and LSCOx families is that due to Sr doping in LSCOx, this material contain a large level of inherent disorder potentially diminishing the resonance peak. This is because by introducing disorder into optimally doped YBCO6+x in a controlled fashion (1% or less of Zn and Ni impurities), large effect on resonance [98] are observed. Finally it should be mentioned that similar dispersions observed [99] for the SC phases of optimally doped LSCOx and YBCO suggests the magnetic excitations in these HTSC cuprates are of universal character and that the differences may be caused by the differences in the charge states[21].

3.4. Pseudogap

For underdoped samples, polarized-neutron scattering measurements [27,60] give evidence for the pseudogap effect. This effect is characterized by a strong decrease of the imaginary part of the spin susceptibility at $\mathbf{Q}=(\pi, \pi)$ starting at a temperature well above T_c (for an example see Fig. 10) on cooling. The low energy spin susceptibility vanishes completely only at temperatures below T_c indicating the opening of the SC gap in the superconducting state. While for an overdoped sample, the susceptibility measured by neutron scattering drops at temperatures only below T_c. This demonstrates that the disappearance of the pseudogap effect on entering the overdoped regime results mainly from the very fast disappearance of the AF correlations for doping

21. There are other differences in the detailed behaviour of YBCO6+x compared to LSCOx. For example, while a glass phase is observed for lightly doped LSCOx, such behaviour is under debate for very underdoped YBCO6+x superconductors [100] where the spin spectrum consists of commensurate AF elastic and inelastic scattering with finite correlation lengths.

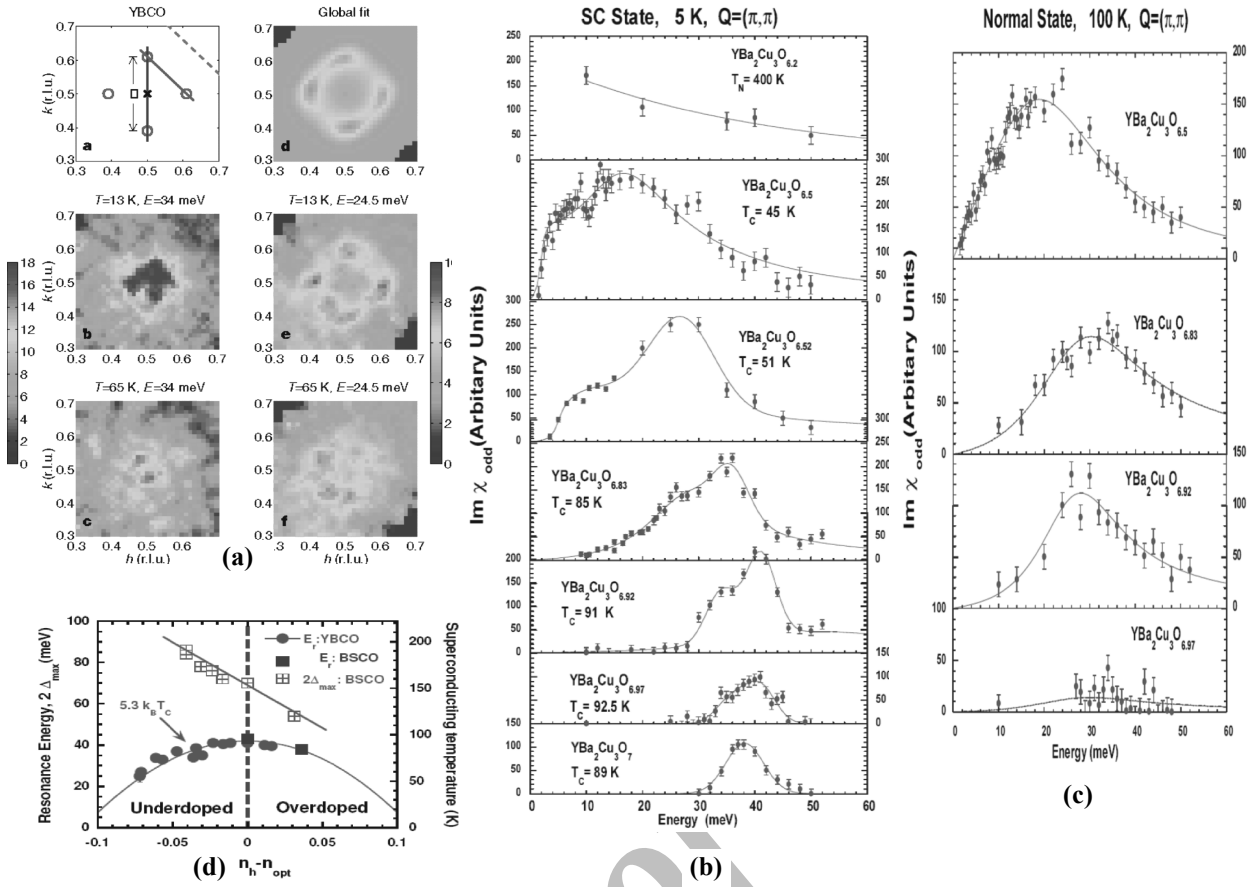

Figure 9. (a) Magnetic scattering from YBCO6.6 above and below T_c at 34 and 24.5 meV in the two dimensional reciprocal space. At the lower energy, an incommensurate response appears at (π,π) position. From Ref. [81], (b) Imaginary part of the acoustic spin susceptibility at 5 K in the SC state for six oxygen contents in YBCO6+x. At the top, the spin waves scattering of the undoped parent compound at 8 K is displayed for comparison. From Ref. [60], (c) Imaginary part of the acoustic spin susceptibility at 100 K in the normal state for four oxygen contents in YBCO6+x in the same units as those of panel (b) using standard phonon calibration [50]. Using further measurements [91], 100 counts in the vertical scale would roughly correspond to $\chi_{max} \sim 350\ \mu_B^2$/eV in absolute units. Lines are fit by a damped Lorentzian function $\mathrm{Im}\,\chi(q,\omega) = \frac{\chi_q \omega \Gamma}{(\omega-\omega_{pg})^2+\Gamma^{-2}}$ where ω_{pg} (~28 meV in heavily-doped samples) is the characteristic energy corresponding to the pole of the spin susceptibility. From Ref. [60], (d) Doping dependence of the resonance energy at (π,π) in YBCO6+x and BSCCO. The doping level has been determined through the empirical relation T_c/T_c^{max}=1-82.6$(n_h-n_{opt})^2$ with n_{opt} identified as a hole doping level of 16%. The red full curve shows the doping dependence of $5.3T_c$. Twice the maximum SC gap as measured in BSCCO by ARPES is also shown. From Ref. [92].

levels larger than optimal doping, leading the electronic system to recover a more conventional metallic character.

Spin-lattice relaxation measurements measured by NMR experiments also indicate the presence of the pseudogap behavior. For a comparison in figure 10(b), two examples of temperature evolution of the imaginary part of susceptibility obtained by neutron scattering at low energy (10 meV) for two samples with oxygen contents 6.92 (slightly underdoped with $T_c \approx 91$ K) and 7 (slightly overdoped with $T_c \approx 92.0$ K) and also values of the $1/^{63}T_1T$ as a function of temperature is shown [101]. The low energy part of the spin susceptibility displays a maximum around $T^* \approx 120$-130 K well above T_c for underdoped sample whereas the maximum for overdoped sample occurs just above T_c. Because this drop is absent in the overdoped regime, it is ascribed to the AF correlations.

There are many theoretical attempts to explain the pseudogap phenomenon including AF fluctuations, stripes, spin-charge separation, preformed pairs, and quantum critical point (including d-density wave) models. Perhaps one of the main challenges facing the theorists is that the real experimental pseudogap phase diagram is still under debate. This is mainly because the crossover temperatures are somewhat sample dependent, a slightly different definition is employed to determine the crossover temperatures by different authors, the crossover temperatures become too close to (or perhaps less than) T_c in the optimally doped and overdoped

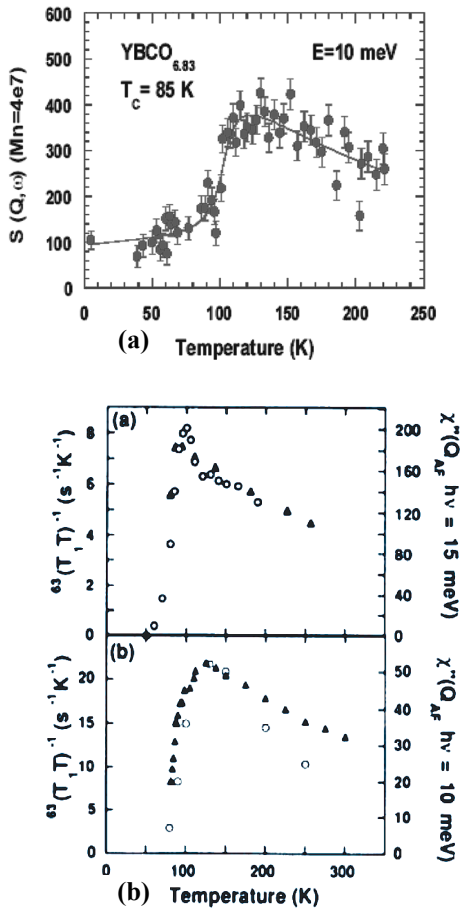

Figure 10. (a) Temperature dependence of peak intensity at low energy in YBCO6.83. From Ref. [60], (b) Comparison between the temperature dependence of $(^{63}T_1T)^{-1}$ (♠) and $\chi''(Q_{AF}, \omega)$ (o) at a small fixed value of ω in (a) YBCO7 overdoped and (b) YBCO6.92 underdoped samples. From Ref. [101].

regimes of the phase diagram and also because different experimental probes investigate different consequences associated with the pseudogap. Nevertheless, it seems that there are [102] mainly two school of thoughts with respect to the pseudogap which are shown in figure 11. In (a), T^* falls from a high value (comparable to the exchange energy) at low doping and falls abruptly to zero at a critical doping point (identified at p=0.19 while optimal doping is at p=0.16). In this case, the pseudogap is necessarily independent and competing with superconductivity and could implicate a quantum critical point. In (b), T^* merges with T_c on the overdoped side [102]. This may suggest that the pseudogap is the result of some form of precursor pairing which evolves into the phase coherent SC state at T_c. This scenario is also implicated by strong correlation spin-charge separation models. The origin of pseudogap is still under debate.

3.5. Very high energy excitations

Recently, neutron scattering experiments have been performed at energies much above the resonance for

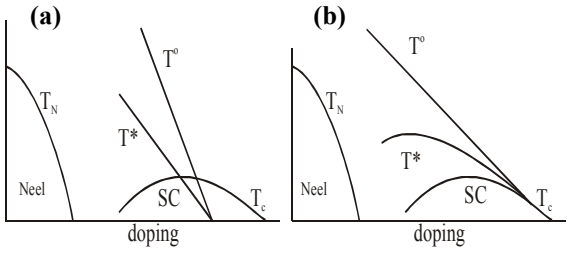

Figure 11. Two scenarios for the pseudogap phase. In (a) T^* (and often a higher T^o associated with a maximum in uniform susceptibility) falls abruptly to zero at a critical doping, p=0.19. In (b) T^* (T^o) merges with T_c on the overdoped side.

YBCO6+x [99,103]. An upward dispersion from the resonance is observed, resulting in the "hourglass" structure in an energy-momentum diagram with the largest intensity belonging to the commensurate resonance peak at the "neck" of the hourglass (see figure 12). The excitations at these very high energies disperse away from the AF wavevector (π,π) in a manner which is reminiscent of the spin waves of the undoped system [99].

Neutron scattering experiments on LBCO0.125, which exhibits static charge and spin stripes below 50 K and a greatly suppressed T_c also indicates [96] an hourglass-type dispersion, remarkably similar to that of underdoped YBCO6+x. In particular, the incommensurate scattering which was previously believed to be dispersion less now exhibits downward dispersion [104]. The same phenomenon is also seen in optimally doped LSCOx [99]. This results in a picture of a universal hourglass-shaped spectrum, which is common to LSCOx and YBCO families despite the absence of resonance peak in LSCOx. The high energy excitations appear common while the major difference seems to be in the rearrangement of spectral weight at low energy. This universality supports the picture that all the cuprates share the same short-distance and high energy physics.

3.6. Stripes

The origin of incommensurate spin fluctuations (stripes) occurring as a result of hole doping into the CuO_2 can be explained by a variety of models. In a simple picture for stripes, doped holes into an AF insulator form a fluctuating array of "topological defects" (metallic stripes). The motion of holes exhibits a self-organized quasi-1D electronic character [105,106]. Figure 13 schematically shows spin and charge separation with the spin residing in the AF stripes.

Since the incommensurate response develops suddenly as the metallic compositions are encountered, it might be a manifestation of the Fermi surface, i.e. Fermi-surface nesting. Incommensurate peaks in the dynamical susceptibility occur quite naturally for a 2D square lattice metal away from half filling and can be calculated on the basis of a tight binding model of the band structure [84,107]. Although this explanation leads to a simple interpretation of the effects of superconductivity on the spin fluctuations, no detailed agreement between

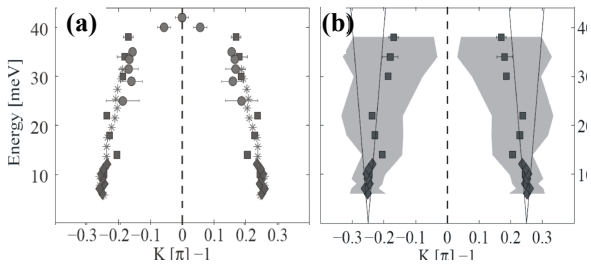

Figure 12. (a) Comparison of incommensurate peak position, δ, for the SC phases of optimally doped LSCOx (squares) and YBCO6.85 (circles), and half the wavevector of the electronic excitations (stars) observed along the (1, 0) direction in $Bi_2Sr_2CaCu_2O_{8+x}$ using STM, (b) Dispersion of the excitations in LSCOx. Shaded regions represent the fitted FWHM. Solid lines show the spin-wave velocity of undoped LCO4 with $J_{\parallel}$=156 meV. From Ref. [99].

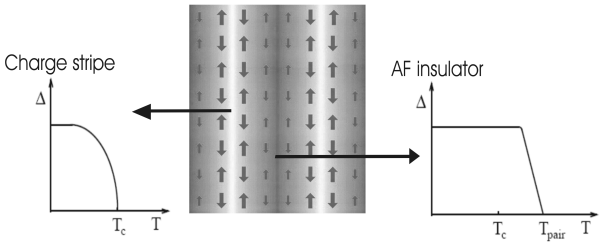

Figure 13. (middle) Schematic picture of a stripe phase with the arrows represent the magnetic or spin order, and the grey scale represents the local charge density. Regions of high charge density (stripes) lie between largely undoped regions, where the spin order is much the same as in the undoped antiferromagnet. The stripes shown lie along the direction of the nearest-neighbor bonds ("vertical" stripes); when the stripes lie at 45° to this axis, they are said to be "diagonal". From Ref. [117]. The figures on the sides show the associated temperature dependence of spin-pairing and SC coherence.

the experiments and calculations in either the normal orSC state are yet available. Models that start with the AF parent compound and introduce frustration with the holes can also lead to incommensurate instabilities [108]. An alternative view is that the incommensurate peaks are a consequence of commensurate AF correlations within stripes determined by the ordering of the holes [106,109]. Static charge[22] and spin ordering of this type occurs in doped La_2NiO_4, Nd doped LSCOx, and also recently observed in LBCO0.125 [104]. This suggests that there are low-lying SDW fluctuations which are almost ready to condense (the static SDW order is stabilized by Zn doping [112] near x=1/8 [113], and in oxygen-doped systems [114]). As mentioned for SC LSCOx there is no static order and attempts to observe charge peaks related to the incommensurate magnetic peaks have not been successful yet.

In the LSCOx family there is a marked suppression of T_c near x=1/8. This suppression is particularly strong with Ba doping, and T_c is completely destroyed if some Nd is substituted for La, as in $La_{1.6-x}Nd_{0.4}Sr_xCuO_4$ for x=1/8. Static SDW and charge density wave (CDW) order were discovered [83] in this system below about 50 K[23]. The period of the S/CDW are eight and four lattice constants, respectively. The static order is modeled by a stripe picture in which holes are concentrated in charge stripes with a period of four separated by spin-ordered regions with antiphase domain walls. It is tempting to interpret the low energy SDW observed in LSCOx as a slowly fluctuating form of stripe order, even though the associated charge order has not yet been seen. The most convincing argument for this interpretation comes from the observation that over arange of doping x=0.06 to x=0.125 the observed incommensurability δ is given precisely by the stripe picture, i.e., δ=x. The stripe phase explains the tendency of T_c to be suppressed near a doping of 1/8 hole per Cu atom, where stripe periodicity becomes commensurate with the lattice spacing. However, δ saturates at approximately 1/8 for $x \geq 0.125$, see figure 6(d). Since in this interpretation the charge stripe must be incompressible leading to a charge insulator, it is difficult to reconcile this picture with the fact that LSCOx is metallic and SC in the same doping range.

An important question with respect to stripe is its relation with the exotic properties of HTSC cuprates such as superconductivity itself or the pseudogap phase in underdoped materials. There have been attempts to use the stripe picture to explain HTSC cuprate properties. For example, in stripe models for pseudogap, T^o marks the crossover temperature at which stripes become well defined and correspondingly local AF correlations develop in the insulating regions. T^* marks the temperature scale at which a spin-gap develops in the stripes and pairing behaviour emerges, see figure 13. The mobile holes on an individual stripe acquire the spin-gap via pair hopping between the stripe and its environment. From quantum mechanical arguments one expects fluctuating stripes in order for superconductivity to happen since a fixed, parallel arrangement of stripes would pin down all the charges in material creating an insulator. This is consistent with neutron scattering results [83] on La-compounds in which static stripes are observed only when they are pinned (by Nd-doping). However, as mentioned there are experimental reports [114,116] on oxygen-doped La-compounds suggesting the presence of static stripes. In a separate attempt, a stripe model of underdoped HTSC is proposed [105,106] based on spinon superconductivity. Spinons are neutral fermionic excitations which appear in 1D systems. It is argued that the spinon superconductivity occurs on charge stripes in CuO_2 planes at $T_{pair}>T_c$. Spinons create pairs on stripes because

22. Recently the new technique of resonant X-ray scattering has led to a direct observation of the charge order in LBCO0.125, rather than inferring it from a combination of spin structure and lattice distortion [110]. For a recent review see Ref. [111].

23. Nd substitution in this system alters the tilt of the CuO_6 octahedra from an orthorhombic arrangement to a low-temperature tetragonal (LTT) phase, encouraging stripe order to rotate into an orientation parallel to the CuO_2 square-planar array and lock into static order [115], see figure 6(e).

of the existence of a large spin-gap in AF domains due to AF correlations [105,106]. The coherent state of the spinon superconductivity is established below T_c by the Josephson coupling between charge stripes carrying the spinon superconductivity.

Although there is now no doubt that stripe excitations occur in the cuprates and that statically ordered stripes suppress superconductivity, whether the stripes are static or fluctuating, if superconductivity and static magnetic order (fixed stripes) coexist or whether stripes help produce superconductivity are still under debate both experimentally and theoretically. It is also hard to see how stripes produce the d-wave symmetry of the pseudogap. It is still not clear whether or not "melted" stripes provide a good description of the underdoped cuprates and a mechanism for the superconductivity, or whether some more conventional Fermi liquid based model is at play [118].

4. Conclusions

The magnetic properties of HTSC cuprates have been studied extensively since their discovery twenty years ago. Among experimental probes, neutron scattering has proven to play a unique role due to special characteristics of the neutron (which allows measurements of spin dynamics at finite momentum with good energy and momentum resolution). The practical difficulties in these experiments arising from large energy scales, weak $S=1/2$ cross-section, and (for metallic samples) short characteristic length scales in HTSCs have forced scientists to put intense efforts in crystal growth methods. Recent advances in the state of the art in inelastic neutron scattering instrumentation and major progress in growth of large high quality and pure single crystals have allowed inelastic and elastic neutron scattering studies for almost all doping concentrations in the phase diagram. Neutron scattering experiments on HTSC cuprates have confirmed that conventional spin wave theory can well describe the antiferromagnetically ordered insulators cuprates. Although doping into the insualting parent compound results in the destruction of long range AF order as well as new properties, such as scaling behavior, the magnetic spectrum still exhibits a behaviour which is reminiscent of the spin waves. Metallic HTSC cuprates exhibit a low energy incommensurate response. This response is different from the insulators and is affected by the SC transition significantly. Higher energy response shows less significant changes with doping and temperature. Although all these properties are more or less similar in LSCOx and YBCO6+x families, one major difference is the (π, π) resonance which has only been seen in YBCO6+x. Further search for a commensurate resonance in LSCOx is required in order to confirm whethere neutron resonance is a generic property of all HTSC materials. Although there is still no microscopic theory for HTSC, the occurrence of strong and doping dependent AF fluctuations along with their close link to the unusual physical properties of HTSC cuprates and with T_c itself naturally suggest an electron-electron origin for the SC pairing is at play. As better quality samples are becoming available and experimental techniques are improving, intrinsic properties of HTSC materials will be determined more precisely. These may reveal which of the proposed models describe HTSCs, or may lead to a new model with new concepts in condensed matter physics for these exotic materials.

The author would like to thank M. Akhavan, B.W. Statt, Z. Tun, and W.J.L. Buyers for useful discussions.

References

1. H K Onnes, Akad van Wetenschappen (Amsterdam) **14** (1911) 113; *ibid* **14** (1911) 818. Historical references found at: C J Gorter, *Rev. Mod. Phys*. **36** (1964) 1.
2. M Tinkham, "*Introduction to superconductivity*", McGraw-Hill, 1996; J R Schrieffer, Theory of superconductivity, Advanced Book Classics, Perseus Books, Reading, 1999; P G de Gennes, "*Superconductivity in metals and alloys*", Addison-Wesley, Reading, 1989.
3. W Meissner, R O Ochsenfeld, *Naturwiss*. **21** (1933) 787.
4. J Bardeen, L N Cooper and J R Schrieffer, *Phys. Rev*. **108** (1957) 1175.
5. J G Bednorz and K A Muller, *Z. Phys*. B **64** (1986) 189.
6. M K Wu et al., *Phys. Rev. Lett*. **58** (1987) 908.
7. Hand book of superconductivity, ed. C P Pool, JR., Academic Press, 2000.
8. W E Pickett et al., *Science* **255** (1992) 46; G C Asomba, *Physica* C **245** (1995) 355; G C Asomba, *Physica* C **244** (1995) 271; J D Fan and Y M Malozovsky, *Physica* C **364-365** (2001) 50.
9. G Blatter et al., *Rev. Mod. Phys*. **66** (1994) 1125; R Wördenweber, *Rep. Prog. Phys*. **62** (1999) 187.
10. J Ruvalds, *Supercond. Sci. Technol*. **9** (1996) 905; E Dagotto, *Rev. Mod. Phys*. **66** (1994) 763.
11. H Kontani et al., *Phys. Rev*. B **59** (1999) 14723 and references therein.
12. D Esteve et al., *Europhys. Lett*. **3** (1987) 1237; C E Gough et al., *Nature* **326** (1987) 855.
13. J R Kirtley et al, *Nature Phys*. **2** (2006) 190; C C Tsuei and J R Kirtley, *Rev. Mod. Phys*. **72** (2000) 969.
14. P A Lee et al, *Rev. Mod. Phys*. **78** (2006) 17.
15. B Batlogg et al, *Physica* C **235** (1994) 130.
16. N Hussey, *Adv. Phys*. **51** (2002) 1685; N Hussey et al., *Nature* **425** (2003) 814.
17. T Timosk, B W Statt, *Rep. Prog. Phys*. **62** (1999) 61.
18. G L Squires, "*Introduction to the theory of thermal neutron scattering*", Dover, New York, 1996; G E Bacon, Neutron Diffraction (Oxford U.P., Oxford,

1975), 3rd ed
19. W Gavin Williams, "*Polarized Neutrons*", Oxford, New York, 1988
20. S W Lovesey, "*Theory of neutron scattering from condensed matter*", Oxford, New York, 1984.
21. G Shirane et al., "*Neutron scattering with a triple-axis spectrometer*", Cambridge University Press, 2002.
22. R M White, "*Quantum theory of magnetism*", Springer Ser. Solid-State Sci., **32**, Springer, Berlin, (1983).
23. D Vaknin et al., *Phys. Rev. Lett*. **58** (1987) 2802.
24. S Mitsuda et al., *Phys. Rev*. B **36** (1987) 826.
25. D Vaknin et al., *Phys. Rev*. B **41** (1990) 1926.
26. M A Kastner et al., *Phys. Rev*. B **38** (1988) 6636.
27. L P Regnault et al., in Neutron scattering in layered copper-oxide superconductors, ed. A Furrer, Vol. **20** of Physics and chemistry of materials with low-dimensional structures, Kluger Academic Publishers, (1998) 85.
28. S M Hayden, in Ref. [27], p. 135.
29. J M Tranquada et al., *Phys. Rev*. B **40** (1989) 4503.
30. S M Hayden et al., *Physica* B **241-243** (1998) 765.
31. R R P Singh, *Phys. Rev*. B **39** (1989) 9760.
32. I Igarashi, *Phys. Rev*. B **46** (1992) 10763; *ibid*, *J. Phys*.: *Condens. Matter* **4** (1992) 10265.
33. G Shirane et al., *Phys. Rev. Lett*. **59** (1987) 1613; Y Endoh et al., *Phys. Rev*. B **37** (1988) 7443.
34. K Yamada et al., *Phys. Rev*. B **40** (1989) 4557.
35. G Aeppli et al., *Phys. Rev. Lett*. **62** (1989) 2052.
36. S M Hayden et al., *Phys. Rev*. B **42** (1990) 10220.
37. S M Hayden et al., *Phys. Rev. Lett*. **67** (1991) 3622.
38. S M Hayden et al., *Phys. Rev. Lett*. **76** (1996) 1344.
39. D R Grempel, *Phys. Rev. Lett*. **61** (1988) 1041.
40. S Tyc et al., *Phys. Rev. Lett*. **62** (1989) 835.
41. M F Collins, "*Magnetic Critical Scattering*", 1989, Oxford University Press, Oxford.
42. B Keimer et al., *Phys. Rev*. B **46** (1992) 14034; B. Keimer et al., *Phys. Rev*. B **45** (1992) 7430.
43. S Chakravarty et al., *Phys. Rev*. B **39** (1989) 2344; P Hasenfratz and F Niedermayer, *Phys. Lett*. B **268** (1991) 231.
44. R J Birgeneau et al., *J. Phys. Chem. Solids* **56** (1995) 1913.
45. D R Harshman et al., *Phys. Rev*. B **38** (1988) 852; B J Sternlieb et al., *Phys. Rev*. B **41** (1990) 8866; N Hasselmann et al., *Phys. Rev*. B **69** (2004) 014424.
46. C M Varma et al., *Phys. Rev. Lett*. **63** (1989) 1996.
47. J Rossat-Mignod et al, *J. Phys. (Paris) Colloq*. **49** (1988) C8-2119; M J Jurgens et al., *Physica* B **156-157** (1989) 846; J Rossat-Mignod et al., *Physica* C **162-164** (1989) 1269.
48. J Rossat-Mignod et al., *Physica* C **185-189** (1991) 86; P Bourges et al., *Europhys. Lett*. **38** (1997) 313; C Stock et al., *Phys. Rev*. B **69** (2004) 014502.
49. H A Mook et al., *Phys. Rev. Lett*. **70** (1993) 3490.
50. H F Fong et al., *Phys. Rev*. B **54** (1996) 6708.
51. Ruixing Liang et al, *cond-mat*/0510674.
52. J M Tranquada et al., *Phys. Rev. Lett*. **60** (1988) 156; P Burlet et al., *Physica* C **153-155** (1988) 1115.
53. K Segawa and Y Ando, *Phys. Rev. Lett*. **86** (2001) 4907; H Alloul et al., *Phys. Rev. Lett*. **63** (1989) 1700; K Conder, "*Materials Science and Engineering*", R **32** (2001) 41; A Goto et al., *J. Phys. Soc. Jpn*. **65** (1996) 3043.
54. J Rossat-Mignod et al., "*in Selected topics in superconductivity*", Frontiers in solid state sciences, Vol. 1, eds. L C Gupta and M S Multani, World Scientific, 1993, p. 265.
55. S Shamoto et al., *Phys. Rev*. B **48** (1993) 13817.
56. D Reznick et al., *Phys. Rev*. B **53** (1996) R14741.
57. J Rossat-Mignod et al., *Physica* B **169** (1991) 58.
58. S M Hayden et al., *Phys. Rev*. B **54** (1996) R6905.
59. O K Anderson et al., *J. Phys. Chem. Solids* **56** (1995) 1573.
60. P Bourges, in "*The gap symmetry and fluctuations in high-T_c superconductors*", eds. J Bok *et al*, Plenum Press, 1998, p. 349; H F Fong et al., *Phys. Rev*. B **61** (2000) 14773.
61. G Aeppli et al., *Science* **278** (1997) 1432.
62. T R Thurston et al., *Phys. Rev*. B **40** (1989) 4585.
63. S-W Cheong et al., *Phys. Rev. Lett*. **67** (1991) 1791.
64. T E Mason et al., *Phys. Rev. Lett*. **68** (1992) 1414.
65. T R Thurston et al., *Phys. Rev*. B **46** (1992) 9128.
66. D Reznik et al., *Nature* **440** (2006) 1170.
67. K Yamada et al., *Phys. Rev*. B **57** (1998) 6165.
68. R J Birgeneau et al., *Phys. Rev*. B **39** (1989) 2868; G Shirane et al., *Phys. Rev. Lett*. **63** (1989) 330.
69. S Petit et al., *Physica* B **234-236** (1997) 800.
70. M Matsuda et al., *Phys. Rev*. B **62** (2000) 9148.
71. D R Noakes et al., *Phys. Rev. Lett*. **65** (1990) 369.
72. H Sato, and K Maki, *Int. J. Magn*. **6** (1974) 183.
73. S Sachdev and J Ye, *Phys. Rev. Lett*. **69** (1992) 2411; A Millis et al., *Phys. Rev*. B **48** (1993) 7183; C Castellani et al., *J. of Phys. and Chem. of Solids* **59** (1998) 1694; A. Chubukov et al., *Phys. Rev*. B **49** (1994) 11919.
74. T E Mason et al., *Phys. Rev. Lett*. **77** (1996) 1604.
75. M Kofu et al., *Phys. Rev*. B **72** (2005) 064502; K. Yamada et al., *Phys. Rev. Lett*. **75** (1995) 1626.
76. Y Zha et al., *Phys. Rev*. B **47** (1993) 9124.
77. T E Mason et al., *Phys. Rev. Lett*. **71** (2003) 919.
78. J M Tranquada et al., *Phys. Rev. Lett*. **64** (1990) 800; H. Chou et al., *Phys. Rev*. B **43** (1991) 8690.
79. S. Pailhes et al., *Phys. Rev. Lett*. **93** (2004) 167001.
80. P Dai et al., *Phys. Rev*. B **63** (2001) 054525; M Arai et al., *Phys. Rev. Lett*. **83** (1999) 4100.
81. H Mook et al., *Nature* **395** (1998) 580.
82. For a discussion about the importance of these kinds of inhomogeneity see E Dagotto, Sceince **309** (2005) 257.
83. J M Tranquada et al., *Nature* **375** (1995) 561.
84. Q Si et al., *Phys. Rev*. B **47** (1993) 9055.
85. A V Balatsky and P Bourges, *Phys. Rev. Lett*. **82** (1999) 5337.
86. T Tanamoto et al., *J. Phys. Soc. Japan* **62** (1993) 1445; G. Stemmann et al., *Phys. Rev*. B **50** (1994) 4075.
87. M R Norman and C Pepin, *Rep. Prog. Phys*. **66**

(2003) 1547.
88. F Onufrieva and J M Rossat-Mignod, *Phys. Rev*. B **52** (1995) 7572; P Monthoux, and D J Scalapino, *Phys. Rev. Lett*. **72** (1994) 2131; N Bulut, and D J Scalapino, *Phys. Rev*. B **53** (1996) 5149; D Z Liu et al., *Phys. Rev. Lett*. **75** (1995) 4130.
89. S-C Zhang, *Science* **275** (1997) 1089.
90. H F Fong et al., *Phys. Rev. Lett*. **75** (1995) 316.
91. Ph Bourges et al., *Phys. Rev*. B **56** (1997) R11439.
92. Ph Bourges et al., *Physica* C **424** (2005) 45.
93. P Bourges et al., *Science* **288** (2000) 1234.
94. Y-J Kao et al., *Phys. Rev*. B **61** (2000) R11898; M R Norman, *Phys. Rev*. B **61** (2000) 14751; J Brinckmann and P A Lee, *Phys. Rev*. B **65** (2002) 014502; F Onufrieva and P Pfeuty, *Phys. Rev*. B **65** (2002) 054515.
95. H He et al., *Science* **295** (2002) 1045.
96. J M Tranquada et al., *Nature* **429** (2004) 534.
97. D K Morr and D Pines, *Phys. Rev. Lett*. **81** (1998) 1086; A Abanov and A V Chubukov, *Phys. Rev. Lett*. **83** (1999) 1652.
98. H F Fong et al., *Phys. Rev. Lett*. **82** (1999) 1939; Y Sidis et al., *Phys. Rev. Lett*. **84** (2000) 5900.
99. N B Christensen et al., *Phys. Rev. Lett*. **93** (2004) 147002.
100. C Stock et al., *Phys. Rev*. B **73** (2006) 100504.
101. M Horvatic et al., *Phys. Rev*. B **47** (1993) 3461.
102. J L Tallon and J W Loram, *Physica* C **349** (2001) 53; J L Tallon et al., *Physica* C **235-240** (1994) 1821.
103. C Stock et al., *Phys. Rev*. B **71** (2005) 024522.
104. M Fujita et al., *Phys. Rev*. B **70** (2004) 104517.
105. V J Emery et al., *Phys. Rev*. B **56** (1997) 6120; J Zaanen, *Science* **286** (1999) 251.
106. V J Emery and S A Kivelson, *Physica* C **209** (1993) 597.
107. N Bulut et al., *Phys. Rev. Lett*. **64** (1990) 2723; P Benard et al., *Phys. Rev*. B **47** (1993) 15217; P B Littlewood et al., *Phys. Rev*. B **48** (1993) 487; T Tanamoto et al., *J. Phys. Soc. Jpn*. **63** (1994) 2739.
108. A Aharony et al., *Phys. Rev. Lett*. **60** (1988) 1330; B I Shraiman, and E I Siggia, *Phys. Rev. Lett*. **62** (1989) 1564.
109. J Zaanen and O Gunnarsson, *Phys. Rev*. B **40** (1989) 7391.
110. P Abbamonte et al., *Nature Phys*. **1** (2005) 155.
111. J M Tranquada, preprint *cond-mat*/9802043.
112. H Kimura et al., *Phys. Rev*. B **59** (1999) 6517.
113. S Wakimoto et al., *Phys. Rev*. B **60** (1999) R769.
114. Y S Lee et al, *Phys. Rev*. B **60** (1999) 3643.
115. J M Tranquada et al., *Phys. Rev. Lett*. **78** (1997) 338.
116. P C Hammel et al., *Phys. Rev*. B **57** (1998) R712; B W Statt et al., *Phys. Rev*. B **52** (1995) 15575.
117. V J Emery et al., *Proc. Natl. Acad. Sci*. **96** (1999) 8814.
118. S A Kivelson et al., *Rev. Mod. Phys*. **75** (2003) 1201.